# METHODS FOR THE LATTICE PHYSICS ANALYSIS OF LWR's

B. L. Darnell
T. D. Beu
G. W. Perry



Topical Report

Tennessee Valley Authority

April 15, 1978

TABLE OF CONTENTS

TABLE OF CONTENTS (Cont.)

LIST OF FIGURES

## ABSTRACT

The methods currently in use at TVA for the lattice physics analysis of LWR's are described in this report. A chapter is devoted to each of the major calculations: the generation of neutron spectra and cross sections, the two-dimensional few-group diffusion theory computation of the flux and power distribution in the assembly, and the change in isotopic concentrations with exposure.



## ACKNOWLEDGMENT

Appreciation is extended to Dr. S. R. Specker for his considerable contributions to the development and application of the methods presented in this report. Other contributors include C. H. Chen, S. L. Forkner, and D. L. Hutson.

# 1. INTRODUCTION

This topical report describes the lattice physics methods in use at the Tennessee Valley Authority. These methods are embodied in a computer program called LATTICE, which TVA has been actively developing for several years. LATTICE consists of several components which perform the various calculations: the computation of the neutron spectra and cross sections, the two-dimensional diffusion theory calculation, the fission product treatment and depletion. The only calculation that is done in a separate program is the generation of macroscopic cross sections for control rods. Although LATTICE evolved from the United Nuclear Corporation code LOCALUX (Reference 1-1), which was a modification of LASER (Reference 1-2), there is now very little similarity to either of these codes.

LATTICE requires as input easily obtained design information such as dimensions, densities, loadings, and number densities. Relatively few number densities are required, since the code calculates fuel and moderator number densities. The output consists of data required by the TVA reactor simulator code, such as the assembly infinite multiplication factor, the two-group constants, the energy release per fission neutron, the xenon thermal microscopic absorption cross section, xenon and control reactivity worths, and the fraction of fissions occurring in uranium. Also printed are many other quantities of interest, such as isotopic concentrations, the fast and thermal spectra, reaction rates, and the assembly local fission power distribution. The methods which TVA has implemented to calculate these parameters are documented in this report.

## CHAPTER 1 REFERENCES


1. R. R. Calabro and J. M. Fiscella, "LOCALUX-4 - A Depletion Program for Multizoned Reactor Assemblies," UNC-5262, 1970.

2. C. G. Poncelet, "LASER - A Depletion Program for Lattice Calculations Based on MUFT and THERMOS," WCAP-6073, 1966.

# 2. CROSS SECTION GENERATION

## 2.1 CROSS SECTION LIBRARIES

### 2.1.1 Epithermal Data

HRG3 (Reference 2-1) is incorporated into the LATTICE code to calculate the epithermal neutron spectrum and the spectrum averaged epithermal cross sections. The epithermal energy range from 10 MeV to the thermal cutoff of 1.855 eV is divided into 62 energy groups, each of lethargy width 0.25. Following is a list of the materials present in the current HRG library.

Table 2-1

List of Materials in the HRG Library

| MATERIAL | ID | SOURCE | ENDF/B MATNO |
|---|---|---|---|
| U-235 | 12 | III | 1157 |
| U-236 | 67 | IV | 1163 |
| U-238 | 13 | IV | 1262 |
| Pu-239 | 14 | III | 1159 |
| Pu-240 | 77 | III | 1105 |
| Pu-241 | 78 | IV | 1266 |
| Pu-242 | 17 | IV | 1161 |
| Gd-155 | 241 | III | 1252 |
| Gd-157 | 243 | III | 1253 |
| Xe-135 | 93 | IV | 1294 |
| Sm-149 | 94 | IV | 1027 |
| Fission Product | 47 | HRG | ---- |
| H-1 | 1 | III | 1148 |
| O-16 | 4 | III | 1134 |
| B-10 | 20 | HRG | ---- |
| Zr-2 | 10 | IV | 1284 |
| SS-304 | 11 | HRG | ---- |

The III or IV in the source column indicates that ENDF/B-III or ENDF/B-IV data is used. The data was processed using the SUPERTOG code (Reference 2-2), modified to write its output in the GAM-I format used by HRG3. The last column gives the ENDF/B material numbers that were

used. HRG in the source column signifies that TVA has not updated the cross section data for that particular material from that included in the HRG library obtained from the Argonne Code Center in 1972. The origin of this data is discussed in Reference 2-1.

There are resonance parameters in the HRG library for U-235, U-238, and Pu-239 for a maximum of 99 resonances each. Other resonances for these materials and all resonances for other materials have been treated assuming infinite dilution with Doppler broadening at 300°K. Resonance contributions are added to the non-resonance cross sections of the material.

Two other comments are in order at this point. First, the data for Zircaloy-2 is also used for Zircaloy-4. Second, cross sections for Gd-154 and Gd-156, while not included in either the epithermal or the thermal library, are programed into LATTICE for use in the calculation of activation rates for the gadolinium depletion chain. Since the macroscopic cross sections of these gadolinium isotopes are small, they are not included in the spectrum calculations.

### 2.1.2 Thermal Data

Thermal neutron spectra are calculated for 35 groups below 1.855 eV using a variation of THERMOS (Reference 2-3). Table 2-2 shows the materials present in the current thermal cross section library. The material with ID 55555 is a lumped fission product with a 1/v 2200 m/sec cross section of 50 barns.

Scattering kernels were generated for hydrogen bound in water using $S(\alpha,\beta)$ data (ENDF/B material number 1002). A special version of the XLACS code (Reference 2-4), developed for TVA by ORNL, was used to process the data. For atoms heavier than hydrogen, an analytic free gas or diffusive model is used, as in FLANGE-II (Reference 2-5). The third column

Table 2-2

List of Materials in the THERMOS Library

| MATERIAL | ID | KERNELS | UPDATED |
|---|---|---|---|
| U-235 | 23592 | 0 | Yes |
| U-236 | 23692 | 0 | No |
| U-238 | 23892 | 0 | Yes |
| Pu-239 | 23994 | 0 | Yes |
| Pu-240 | 24094 | 0 | Yes |
| Pu-241 | 24194 | 0 | Yes |
| Pu-242 | 24294 | 0 | Yes |
| Gd-155 | 20 | 0 | Yes |
| Gd-157 | 2713 | 0 | Yes |
| Xe-135 | 13554 | 0 | Yes |
| Sm-149 | 14962 | 0 | Yes |
| Fission Product | 55555 | 0 | No |
| H | 18 | 6 | Yes |
| O | 168 | 7 | Yes |
| B-10 | 115 | 6 | No |
| Zr | 9140 | 6 | No |
| SS-304 | 30400 | 6 | No |
| Heavy Scatterer | 92940 | 7 | Yes |

indicates the number of scattering kernels present for that material. For all materials with no kernels, the scattering kernel for the heavy scatterer, ID 92940, is used. These kernels were generated using U-238 data and the TVA version of XLACS. A seven in the third column indicates that scattering kernels are present for temperatures of 80, 212, 390, 500, 550, 600, and 1160 degrees F; a six indicates that kernels are present for the first six temperatures listed.

Table 2-2 also indicates whether TVA has updated the cross-section data of the particular material from that in the original LASER library to the ENDF/B-III data. We have made comparisons of the B-10, SS-304, and Zr-2 2200 m/sec absorption cross sections in our library to more authoritative values. For Zircaloy, our value is 3 percent higher than the ENDF/B-IV cross section. Comparison values for the two other materials were directly obtained from, or calculated from values given in,

EPRI-221 (Reference 2-6). The results were that for B-10, there was a 2b out of 3837b difference, and for SS-304, our value was 3 percent higher than the quoted value. These differences cause little error in the calculations and thus are acceptable.

## 2.2 DANCOFF FACTORS

An important aspect of LWR lattice physics methods is the calculation of Dancoff factors which are used in evaluating the resonance integrals of the fuel. Sauer's method (Reference 2-7) for an infinite uniform array of pins is suitable for analyzing PWR's. However, a more detailed calculation is necessary for use in analyzing BWR's due to the presence of water gaps and water holes. Rod dependent Dancoff factors are calculated for BWR's using the DANCOFF JUNIOR routine of Gellings and Sauer (Reference 2-8).

### 2.2.1 Theory

The Dancoff factor accounts for the reduced flux at a fuel rod surface caused by neutron absorption in the lattice surrounding the rod. Since the blackness $\beta$ of a region is the probability that a neutron entering the region is absorbed in that region, the Dancoff factor is equivalent to the blackness of the surrounding "moderator" region.

Referring to Figure 2-1, let $\underline{n}$ be a unit vector directed into the moderator, perpendicular to a fuel rod surface element dS, and let $\underline{\Omega}$ be the direction of a chord in the moderator of length $\ell$. Then $(\underline{\Omega}\cdot\underline{n})$ is the cosine of the angle between $\underline{n}$ and $\underline{\Omega}$. The following three assumptions are made:

a) the fuel rods absorb all incident neutrons,

b) the neutron source distribution in the moderator has no angular or spatial dependence, and

c) the resonances are sufficiently narrow that any scattering collision in the moderator removes the neutron from the energy range of the resonance.

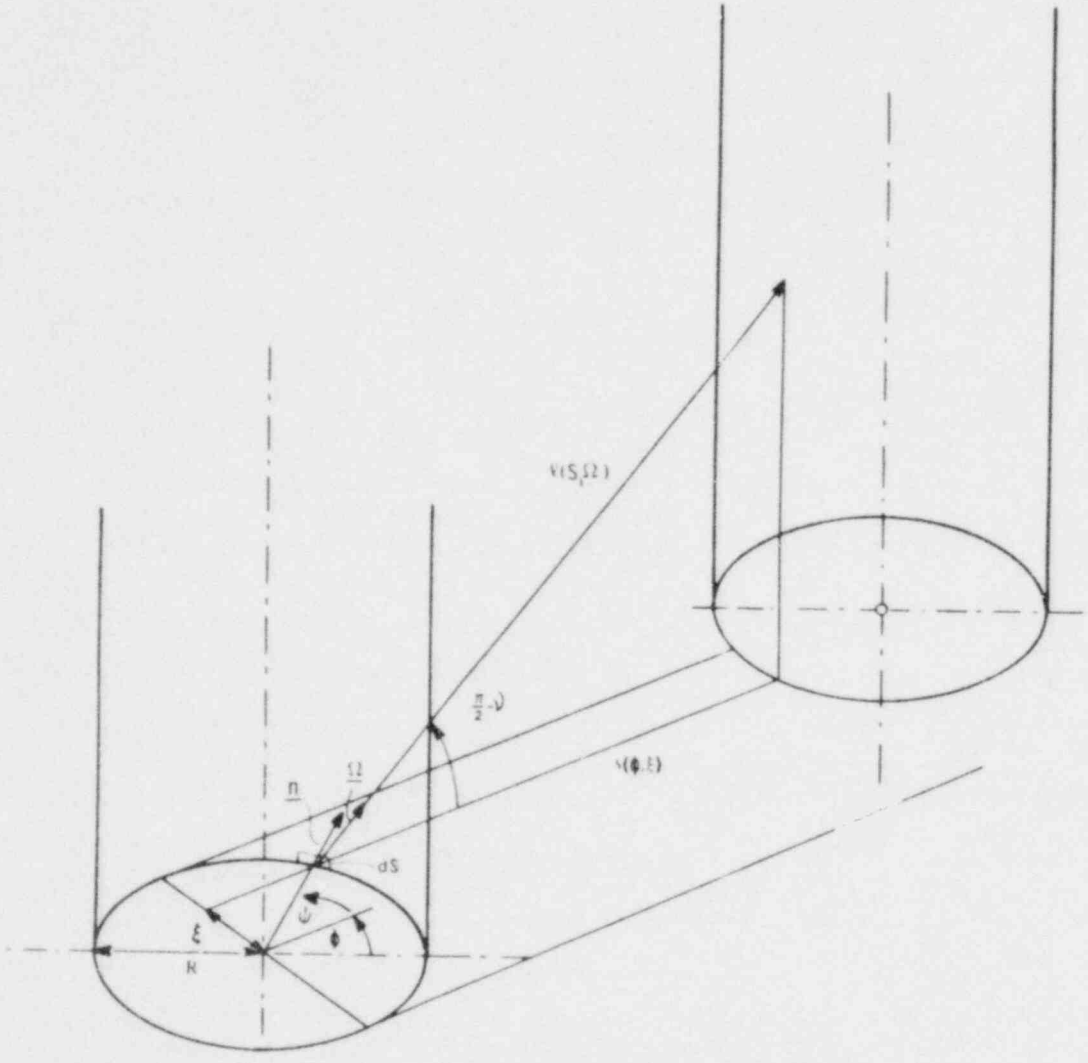


FIGURE 2-1: GEOMETRY FOR CALCULATION OF MODERATOR BLACKNESS

Then the blackness can be written as (Reference 2-8):

$$\beta = 1 - \frac{\iint (\underline{\Omega}\cdot\underline{n}) e^{-\Sigma\ell} d\underline{\Omega} dS}{\iint (\underline{\Omega}\cdot\underline{n}) d\underline{\Omega} dS}, \qquad (\underline{\Omega}\cdot\underline{n}) > 0 \qquad (2\text{-}1)$$

where $\ell$ is a function of S and $\underline{\Omega}$. Define the chord distribution function $f(\ell)$ so that $f(\ell)d\ell$ is the probability that a chord is of length between $\ell$ and $(\ell+d\ell)$:

$$f(\ell)d\ell = \frac{\iint_{\ell=\ell_s} (\underline{\Omega}\cdot\underline{n}) d\underline{\Omega} dS}{\iint (\underline{\Omega}\cdot\underline{n}) d\underline{\Omega} dS}, \qquad (\underline{\Omega}\cdot\underline{n}) > 0 \qquad (2\text{-}2)$$

where $\ell_s$ is the length of the chord of interest (Reference 2-9).

Rewriting Equation (2-1) using Equation (2-2) yields the general expression for the blackness and the Dancoff factor:

$$C = \beta = \int f(\ell)\ (1-e^{-\Sigma\ell})\ d\ell \qquad (2\text{-}3)$$

2.2.2 PWR Method

Sauer (Reference 2-7) approximated the chord distribution function in the moderator as a simple exponential distribution, characterized by the mean chord length $\bar{\ell}$, shifted by a distance t:

$$f(\ell)d\ell = \begin{cases} 0 & \ell < t \\ \exp\left[-\left(\frac{\ell-t}{\bar{\ell}-t}\right)\right] d\left(\frac{\ell-t}{\bar{\ell}-t}\right) & \ell \geq t \end{cases}$$

Substituting this distribution into Equation (2-3) gives the following equation for the Dancoff factor:

$$C = 1 - \frac{e^{-\tau\Sigma\bar{\ell}}}{1+(1-\tau)\Sigma\bar{\ell}} \qquad (2\text{-}4)$$

where

$$\tau = \left\{ \left[ \frac{\pi}{4}\left(1 + \frac{V_m}{V_f}\right)\right]^{\frac{1}{2}} - 1 \right\} \frac{V_f}{V_m} - 0.08 \quad \text{(for a square lattice)},$$

$V_m$ = the volume fraction of the moderator,

$V_f$ = the volume fraction of the fuel, and

$\Sigma$ = the total macroscopic cross section of the moderator.

The moderator is defined as the homogenization of all non-fuel regions.

### 2.2.3 BWR Method

Referring to Figure 2-1, Gellings and Sauer (Reference 2-8) make the following substitutions into Equation (2-2):

$$dS = R\, d\phi\, dz, \quad 0 \leq \phi \leq 2\pi, \quad -\infty < z < \infty$$

$$d\Omega = d\upsilon \sin\upsilon\, d\psi = d\upsilon \sin\upsilon \frac{d\xi}{\sqrt{1-\xi^2}} \qquad \begin{matrix} 0 \leq \upsilon \leq \pi \\ -1 < \xi < 1 \end{matrix}$$

$$(\Omega \cdot n) = \cos\psi \sin\upsilon = \sqrt{1-\xi^2} \sin\upsilon$$

$$\ell = \frac{s(\phi,\xi)}{\sin\upsilon}$$

The first collision blackness becomes

$$\beta = 1 - \frac{\displaystyle\int_{-\infty}^{\infty} dz \int_0^{\pi} \sin^2\upsilon\, d\upsilon \int_0^{2\pi} d\phi \int_{-1}^{+1} \exp\left[-\frac{\Sigma s(\phi,\xi)}{\sin\upsilon}\right] d\xi}{\displaystyle\int_{-\infty}^{\infty} dz \int_0^{\pi} \sin^2\upsilon\, d\upsilon \int_0^{2\pi} d\phi \int_{-1}^{+1} d\xi}$$

or

$$\beta = 1 - \frac{4}{\pi} \int_0^{2\pi} \frac{d\phi}{2\pi} \int_{-1}^{+1} \frac{1}{2} \mathrm{Ki}_3(\Sigma s)\, d\xi \qquad (2\text{-}5)$$

For a $\pi/4$ section,

$$\beta\left(\frac{\pi}{4}\right) = 1 - \frac{4}{\pi} \int_0^{\pi/4} \frac{d\phi}{\pi/4} \int_{-1}^{+1} \frac{1}{2} Ki_3(\Sigma s)\, d\xi \qquad (2\text{-}6)$$

where

$Ki_3(x)$ = Bickley function of order 3

$$\cong \frac{\exp(-x)\,(x^2 + 6.399407x + 5.066719)}{\sqrt{0.6366198x + 1.6211389}\,(x^2 + 6.766116x + 5.066719)}$$

$\Sigma$ = the moderator total macroscopic cross section,

$s(\phi,\xi)$ = the mean chord length in the moderator between the reference rod and the nearest rod in the lattice,

$\phi$ = the angle around the rod, $0 \leq \phi \leq \pi/4$ , and

$\xi$ = the perpendicular distance from the line $\xi_{mn}$ to the point where the chord leaves the surface of the reference rod (Figure 2-2).

Thus the following information is required for the BWR lattice:

a) the distance from the reference rod to the water gaps for each $\pi/4$ direction,

b) a library of the lattice configuration within a $\pi/4$ angle, and

c) the rod type in each rod location.

Once the blackness is calculated for each $\pi/4$ direction, the rod Dancoff factor can be calculated as the sum of the blacknesses. The Dancoff calculation is repeated for each different rod type. For both 7x7 and 8x8 BWR fuel assemblies, we have assumed that the Dancoff factor for any rod more than two rod positions from a water gap is not affected by the gap. The water hole in the 8x8 design is also represented. After rod-by-rod Dancoff factors are calculated, the assembly Dancoff factor is found by averaging the rod-by-rod values.

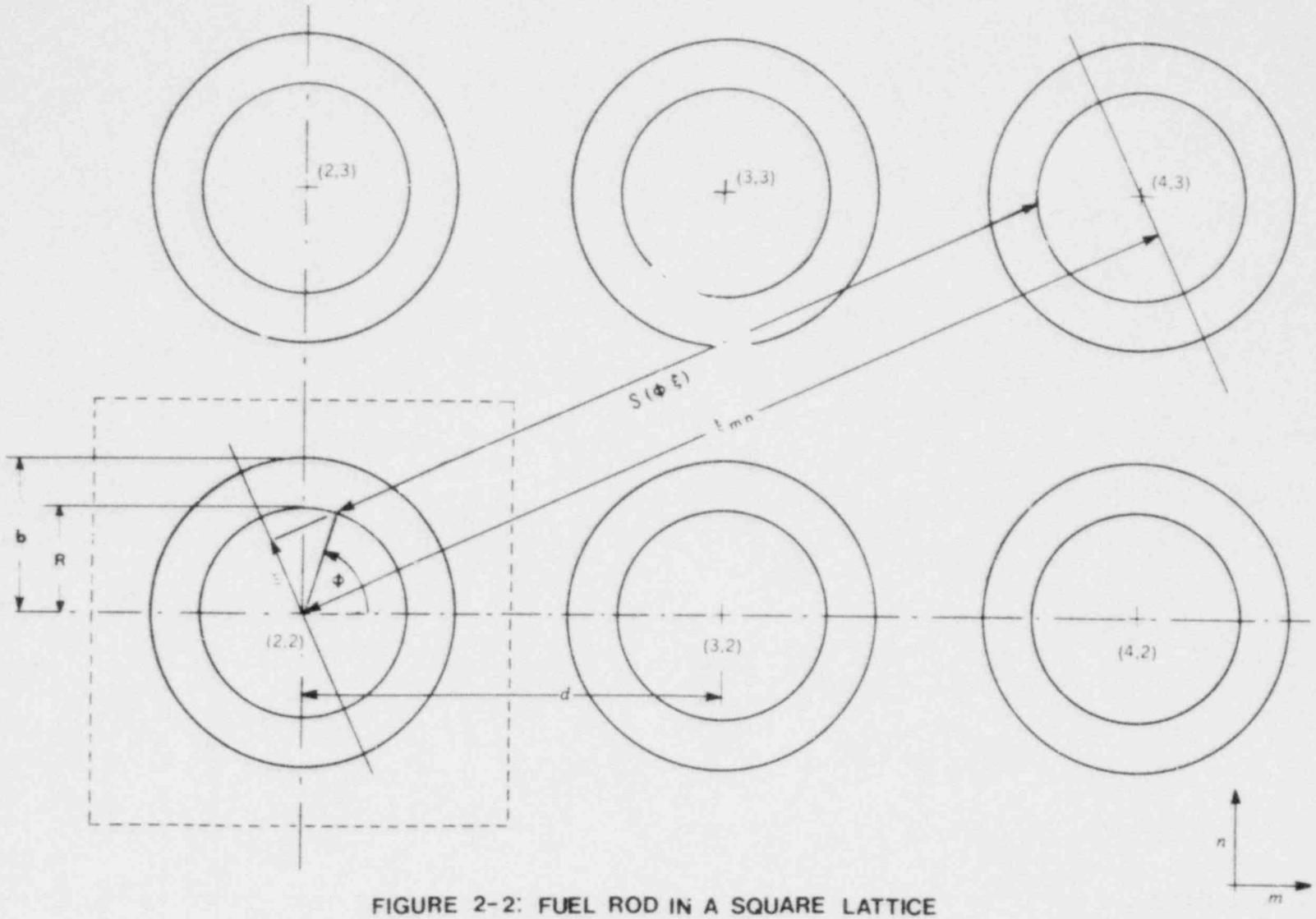


FIGURE 2-2: FUEL ROD IN A SQUARE LATTICE

## 2.3 RESONANCE CALCUATIONS

The method used for the resonance calculations is identical to that used in the HRG3 code. The derivation presented here is adapted from the HRG3 manual (Reference 2-10).

The contribution of a single resonance to the cross section for process x, absorption or fission, of the fine energy group g in an homogenized cell is:

$$\sigma_{x,g} = \frac{\int_{E_g}^{E_{g-1}} \sigma_x(E)\phi(E)dE}{\int_{E_g}^{E_{g-1}} \phi_{cell}(E)dE} \qquad (2\text{-}7)$$

where $\phi(E)$ is the flux spectrum in the absorber region, and $\phi_{cell}(E)$ is the flux spectrum of the homogenized cell. It is assumed that the resonances are isolated and therefore the total resonance contribution to the cross section in an energy group will be the sum of the contributions of the individual resonances within that group.

In practice, it is much simpler to calculate the total number of x processes by a resonance:

$$I_x = \int_0^{\infty} \sigma_x(E)\phi(E)dE \qquad (2\text{-}8)$$

and then find an approximate value for the fraction of x processes which occur in group g:

$$f_{x,g} = \frac{1}{I_x} \int_{E_g}^{E_{g-1}} \sigma_x(E)\phi(E)dE \qquad (2\text{-}9)$$

Thus, Equation (2-7) can be rewritten as

$$\sigma_{x,g} = \frac{I_x \cdot f_{x,g}}{\phi_g} \qquad (2\text{-}10)$$

where $\phi_g$ is the integral of the homogenized cell flux over group g.

The calculation of the quantities in Equation (2-10) for a resolved resonance will now be considered followed by a description of the modifications made in the method when it is applied to the unresolved region.

### 2.3.1 Resolved Resonances

The resonance integral $I_x$ is evaluated using a modification of the method of Adler, Hinman, and Nordheim (AHN method, Reference 2-11) that includes an intermediate resonance approximation for both the resonance absorber and an admixed moderator. The result is

$$I_x = \frac{\sigma_0 \Gamma_x}{E_0} \left[ \beta_{\kappa\lambda} \, J(\xi, \beta_{\kappa\lambda}) + L(\tau_{\kappa\lambda}, \xi, \beta_{\kappa\lambda}) \right] \qquad (2\text{-}11)$$

where $\Gamma_x$ is the level width for process x, $E_0$ is the resonance energy, and

$$\sigma_0 = 2.6035 \times 10^6 \frac{\Gamma_n}{E_0 \Gamma} g \qquad (2\text{-}12)$$

The parameters $\Gamma_n$ and $\Gamma$ are the neutron scattering width and the total width of the resonance, respectively, and g is the statistical spin factor. The Doppler broadening constant $\xi$ is

$$\xi = \frac{\Gamma}{2} \left( \frac{A}{E_0 T} \right)^{\frac{1}{2}} \qquad (2\text{-}13)$$

where T is the temperature in eV and A is the atomic weight in neutron mass units. The parameters $\beta_{\kappa\lambda}$ and $\tau_{\kappa\lambda}$ are determined by the expressions

$$\beta_{\kappa\lambda} = \frac{(\kappa-\lambda)\sigma_m + \lambda\sigma_p}{\sigma_0} \frac{\Gamma}{\Gamma_a + \lambda\Gamma_n} \qquad (2\text{-}14)$$

$$\tau_{\kappa\lambda} = \left[ (\kappa-\lambda)\sigma_m + \lambda\sigma_p \right] N\bar{\ell} \qquad (2\text{-}15)$$

where $\kappa$ and $\lambda$ are the intermediate resonance parameters, N is the lumped nuclear density of the absorber, $\bar{\ell}$ is its equivalent mean chord length

$$\bar{\ell} = \frac{4V}{S(1-C)} \qquad (2\text{-}16)$$

where V and S are the volume and surface area of the absorber region, and C is the Dancoff factor. The parameter $\sigma_p$ is the off-resonance scattering cross section per absorber nuclide of all the atoms in the absorber region:

$$\sigma_p = \sigma_m + \frac{\Sigma_{s,heavy}}{N} \qquad (2\text{-}17)$$

where $\sigma_m$ is the scattering cross section per absorber nuclide of the admixed light atoms

$$\sigma_m = \frac{\Sigma_{s,light}}{N} \qquad (2\text{-}18)$$

The functions $J(\xi,\beta_{\kappa\lambda})$ and $L(\tau_{\kappa\lambda},\xi,\beta_{\kappa\lambda})$ are defined as

$$J(\xi,\beta_{\kappa\lambda}) = \int_0^\infty \frac{\psi(\xi,x)}{\psi(\xi,x) + \beta_{\kappa\lambda}}\, dx \qquad (2\text{-}19)$$

$$L(\tau_{\kappa\lambda},\xi,\beta_{\kappa\lambda}) = \int_0^\infty \frac{[\psi(\xi,x)]^2}{\psi(\xi,x) + \beta_{\kappa\lambda}} P_0 \frac{\tau_{\kappa\lambda}}{\beta_{\kappa\lambda}} \left[ \psi(\xi,x) + \beta_{\kappa\lambda} \right] dx \qquad (2\text{-}20)$$

where

$$x = \frac{2}{\Gamma}(E-E_0)$$

The Doppler function $\psi$ is

$$\psi(\xi,x) = \frac{\xi}{\sqrt{4\pi}} \int_{-\infty}^\infty \frac{dy}{1+y^2} \exp\left[ -\frac{\xi^2}{4}(x-y)^2 \right] \qquad (2\text{-}22)$$

and $P_0$ is the average escape probability from the absorber region. The J and L functions are evaluated through the use of tables.

The method by which Equation (2-11) was obtained is a follows. The AHN method uses the Narrow Resonance (NR) approximation for narrow resonances and the Narrow Resonance Infinite Mass (NRIM) approximation for wide resonances. For absorbing regions containing an admixed moderator, the AHN equations for these two approximations can be combined into a single equation by letting $\lambda = 1$ for NR or $\lambda = 0$ for NRIM. This suggests that an intermediate resonance (IR) approximation, which assigns $\lambda$ a value between 0 and 1, would give improved results. The IR method used is that of Ishiguro (Reference 2-12), who also extended the method to include admixed moderators through the introduction of additional parameters. However, only a single admixed moderator (oxygen), characterized by the parameter $\kappa$, is assumed to be present in the absorber (fuel) and higher order refinements of Ishiguro are neglected. Equation (2-11) is the result when $\kappa$ is introduced.

The IR parameters are evaluated from expressions which depend on the resonance integral itself. However, it is assumed that this dependence is sufficiently weak that a simplified version of the resonance integral can be used for this purpose. It is also assumed that unbroadened cross sections can be used to evaluate the IR parameters. Using the Wigner rational approximation to the escape probability $P_0$,

$$P_0 = \frac{\sigma_e}{\sigma_t + \sigma_e} \qquad (2\text{-}23)$$

where $\sigma_e = 1/(\bar{\ell}N)$ is an effective cross section for escape, and expressing $P_0$ in terms of the quantities in Equation (2-11) yields

$$\beta_{\kappa\lambda}\, J(\xi,\beta_{\kappa\lambda}) + L(\tau_{\kappa\lambda},\xi,\beta_{\kappa\lambda}) = \beta'_{\kappa\lambda}\, J(\xi,\beta'_{\kappa\lambda}) \tag{2-24}$$

where

$$\beta'_{\kappa\lambda} = \beta_{\kappa\lambda} + \frac{\beta_{\kappa\lambda}}{\tau_{\kappa\lambda}} = \frac{(\kappa-\lambda)\sigma_m + \lambda\sigma_p + \sigma_e}{\sigma_0} \quad \frac{\Gamma}{\Gamma_a + \lambda\Gamma_n} \tag{2-25}$$

When unbroadened cross sections are used with Equation (2-24) in evaluating the resonance integral $I_x$ and the IR conditions are applied, one finds that $\lambda$ and $\kappa$ are solutions of

$$\lambda = 1 - \frac{\tan^{-1} X_{\kappa\lambda}}{X_{\kappa\lambda}} \tag{2-26}$$

$$\kappa = 1 - \frac{\tan^{-1} Y_{\kappa\lambda}}{Y_{\kappa\lambda}} \tag{2-27}$$

with

$$X_{\kappa\lambda} = \frac{4A}{(A+1)^2} \quad \frac{E_0}{\Gamma} \left(\frac{\beta'_{\kappa\lambda}}{1+\beta'_{\kappa\lambda}}\right)^{\frac{1}{2}} \tag{2-28}$$

$$Y_{\kappa\lambda} = \frac{4A_m}{(A_m+1)^2} \quad \frac{E_0}{\Gamma} \left(\frac{\beta'_{\kappa\lambda}}{1+\beta'_{\kappa\lambda}}\right)^{\frac{1}{2}} \tag{2-29}$$

where $A_m$ is the admixed moderator mass in units of the neutron mass and all other quantities are as previously defined. Equation (2-11) is then evaluated by use of these $\kappa$ and $\lambda$. Note that the AHN assignments of each resonance to either the NR or NRIM approximation are used only in starting the iterative solution of the transcendental equation for $\lambda$.

The Wigner rational approximation and unbroadened cross sections are also used in evaluating $f_{x,g}$ in Equation (2-9). As $f_{x,g}$ was defined, it is the ratio of the two integrals, each with the same integrand but with different limits. Reference 2-13 shows that the integrand in Equation (2-9) is that of $J(\xi,\beta'_{\kappa\lambda})$:

$$\sigma_x(E)\ \phi(E) = \frac{\psi(\xi,x)}{\psi(\xi,x) + \beta'_{\kappa\lambda}}$$

Assume that the resonance cross sections are unbroadened, i.e., that $T \to 0$ implies that $\xi \to \infty$ [see Equation (2-13)]. Then the integral in Equation (2-22) can be evaluated:

$$\psi(\xi,x) = \frac{1}{1 + x^2} \tag{2-30}$$

Substituting the above two equations into Equation (2-9) yields

$$f_{x,g} = \frac{\displaystyle\int_{x_g}^{x_{g-1}} \frac{1}{1 + \beta'_{\kappa\lambda} + \beta'_{\kappa\lambda} x^2}\, dx}{\displaystyle\int_{-\infty}^{\infty} \frac{1}{1 + \beta'_{\kappa\lambda} + \beta'_{\kappa\lambda} x^2}\, dx} \tag{2-31}$$

where

$$x_g = \frac{2}{\Gamma}\ (E_g - E_0) \tag{2-32}$$

These integrals can be evaluated analytically to give

$$f_{x,g} = \frac{1}{\pi} \left\{ \tan^{-1} \left[ x_{g-1} \left( \frac{\beta'_{\kappa\lambda}}{1 + \beta'_{\kappa\lambda}} \right)^{\frac{1}{2}} \right] - \tan^{-1} \left[ x_g \left( \frac{\beta'_{\kappa\lambda}}{1 + \beta'_{\kappa\lambda}} \right)^{\frac{1}{2}} \right] \right\} \tag{2-33}$$

This expression gives a contribution from the resonance integral to every energy group. Since the contribution is very small for groups far from the resonance, the following cutoff procedure is used. Two energies equally distant from the resonance energy $E_0$ are determined such that 90 percent of the resonance integral is between them. The resonance integral is then allocated according to Equation (2-33) to the energy groups

containing the cutoff energies and all intermediate groups. The contribution of the resonance integral to groups outside the cutoff energies is included in the bounding groups.

Note that the value of $f_{x,g}$ depends on the geometry and the scattering properties of the admixed moderator through $\beta'_{\kappa\lambda}$, but because unbroadened cross sections are used, $f_{x,g}$ is not dependent on the temperature.

The final quantity in Equation (2-10) remaining to be evaluated is the group flux $\phi_g$. An equivalent two region model is assumed. For convenience the absorber region will be referred to as "fuel", the other region as "moderator," and the homogenized system as "cell." It is assumed that the cell flux is the volume weighted average of the two region fluxes:

$$\phi_{cell}(E) = \frac{V_{mod}}{V_{cell}} \phi_{mod}(E) + \frac{V_{fuel}}{V_{cell}} \phi_{fuel}(E) \qquad (2\text{-}34)$$

In the resonance calculation, it has been assumed that $\phi_{mod}(E) = 1/E$. Using this assumption with the Wigner rational approximation, the fuel flux becomes

$$\phi_{fuel}(E) = \frac{1}{E} \cdot \frac{\beta'_{\kappa\lambda}}{\Psi(\xi,x) + \beta'_{\kappa\lambda}} \qquad (2\text{-}35)$$

From the homogenization of the nuclide concentrations it follows that $N_{fuel} V_{fuel} = N_{cell} V_{cell}$. With these assumptions,

$$\phi_g = \int_{E_g}^{E_{g-1}} \phi_{cell}(E)dE$$

$$\phi_g = \int_{E_g}^{E_{g-1}} \left[ \frac{V_{mod}}{V_{cell}} \phi_{mod}(E) + \frac{V_{fuel}}{V_{cell}} \phi_{fuel}(E) \right] dE$$

$$= 0.25 - \frac{\pi\Gamma}{2E_0} \frac{N_{cell}}{N_{fuel}} \frac{f_{x,g}}{\sqrt{\beta'_{\kappa\lambda}(1 + \beta'_{\kappa\lambda})}} \qquad (2\text{-}36)$$

2.3.2 Unresolved Resonances

In the unresolved range, Equation (2-10) still applies in principle but is modified in detail. For the unresolved resonances the following assumptions are made:

a) the narrow resonance approximation (i.e., $\kappa = 1$, $\lambda = 1$),

b) the Wigner rational approximation,

c) spatial self-shielding of the resonance is neglected,

d) the absorption and fission widths of each resonance are equal to their averages in the unresolved range (i.e., $\Gamma_a = \langle\Gamma_a\rangle$ and $\Gamma_f = \langle\Gamma_f\rangle$), and

e) the reduced neutron widths, $\Gamma_n^0 = \Gamma_n/E_0$, are distributed according to the Porter-Thomas distribution

$$P(y) = \frac{e^{-y/2}}{\sqrt{2\pi y}}$$

where

$$y = \Gamma_n^0/\langle\Gamma_n^0\rangle$$

As a consequence of the first three assumptions, the resonance integral $I_x^{unres}$ can be calculated once the parameters of a resonance are known, using the approximation given by Equation (2-24) in Equation (2-11) with $\kappa$ and $\lambda = 1$. From Equation (2-36), $\phi_g$ is 0.25; and $f_{x,g}$ can be set to 1 in the fine group in which the resonance appears and 0 otherwise. Then, from Equation (2-10), the contribution of a typical unresolved resonance about $E_0$ to the fine group cross sections is $4I_x^{unres}(E_0)$.

The unresolved resonance integral is found from Equation (2-11) using the above five assumptions:

$$I_x^{unres}(E) = \frac{\sigma_{m,eff}\langle\Gamma_x\rangle}{E_0}\ \bar{J}(E) \qquad (2\text{-}37)$$

where $\bar{J}(E)$ is the J function averaged over the Porter-Thomas distribution:

$$\bar{J}(E) = \int_0^\infty \frac{dy}{\sqrt{2\pi y}}\ J[\xi(y),\beta_{11}'(y)]e^{-y/2}$$

and

$$\sigma_{m,eff} = \sigma_0\beta_{11}' = \sigma_p + \sigma_e$$

An adaptation of the GAM-I procedure is used to evaluate $\bar{J}(E)$ (Reference 2-13). A change of variables is made from y to the Doppler broadening constant:

$$\xi = B + Gy \qquad (2\text{-}38)$$

where

$$B = \frac{\langle\Gamma_a\rangle}{2}\left(\frac{A}{E_0T}\right)^{\frac{1}{2}}$$

$$G = \frac{\langle\Gamma_n^0\rangle}{2}\left(\frac{A}{T}\right)^{\frac{1}{2}}$$

so that the integral becomes

$$\bar{J}(E) = \frac{1}{\sqrt{2\pi G}}\int_B^\infty \frac{d\xi}{\sqrt{\xi-B}}\ J[\xi,\beta_{11}'(\xi)]\ \exp\left[-\frac{(\xi-B)}{2G}\right] \qquad (2\text{-}39)$$

Note that the integrand is singular at $\xi = B$. The singularity can be removed by dividing the range of integration into two parts: from B to $B + \Delta$, and from $B + \Delta$ to $\infty$, where $\Delta$ is a small number arbitrarily

set to 0.00095. Then the contribution of the first range of integration to the integral can be neglected. In addition, little error is introduced when the upper limit of integration is changed from $\infty$ to 1 since the integrand is very small for $\xi > 1$. Therefore, the integral in Equation (2-39) is evaluated from $B + \Delta$ to 1. Simpson's rule is used to perform the integration.

The total contribution of unresolved resonances to the cross section in a fine group is

$$\sigma_{x,g}^{unres} = \int_{E_g}^{E_{g-1}} 4I_x^{unres} \frac{dE}{\bar{D}} \tag{2-40}$$

where $\bar{D}$ is the average level spacing. Then the factor $dE/\bar{D}$ in the above equation is the probability that a resonance occurs in the energy range E to E + dE. Substituting Equation (2-37) into Equation (2-40) yields

$$\sigma_{x,g}^{unres} = 4\sigma_{m,eff} \frac{\langle \Gamma_x \rangle}{\bar{D}} \int_{E_g}^{E_{g-1}} \bar{J}(E) \frac{dE}{E} \tag{2-41}$$

This integral is evaluated by a method that differs from the GAM-I method and is based on the fact that over the unresolved range, $\ln \bar{J}$ can be accurately approximated by a quadratic equation in the lethargy u. To evaluate the coefficients in this quadratic, $\bar{J}$ must be calculated at only three values; two of these, $u_1$ and $u_3$, are chosen to be the lethargies corresponding to the upper and lower energy limits, respectively, of the unresolved range for the nuclide and the third, $u_2$, is chosen midway between them. Expressing the quadratic in terms of the mean lethargy $u_0$ of that portion of fine group g which is in the

unresolved range and substituting into the integral in Equation (2-41) yields

$$\int_{u_g}^{u_{g-1}} \bar{J}(u)du = \bar{J}_0 \int_{u_g}^{u_{g-1}} \exp[a(u-u_0) + b(u-u_0)^2]du$$

Assuming that the quadratic term in the exponent can be expanded,

$$\int_{u_g}^{u_{g-1}} \bar{J}(u)du = \bar{J}_0 \frac{1}{a}(e^d - e^{-d}) + \frac{2b}{a^3}\left[(1-d+\tfrac{1}{2}d^2)e^d - (1+d+\tfrac{1}{2}d^2)e^{-d}\right] \quad (2\text{-}42)$$

where

$$a = 2u_0 b - c$$

$$b = \frac{2}{\Delta^2}(\ln \bar{J}_1 - 2\ln \bar{J}_2 + \ln \bar{J}_3)$$

$$c = \frac{2}{\Delta^2}\left[(u_2+u_3)\ln \bar{J}_1 - 2(u_1+u_3)\ln \bar{J}_2 + (u_1+u_2)\ln \bar{J}_3\right]$$

$$d = \delta_g a/2$$

$$\ln \bar{J}_0 = \frac{2}{(u_1-u_3)^2}\left[(u_0-u_2)(u_0-u_3)\ln \bar{J}_1 - 2(u_0-u_1)(u_0-u_3)\ln \bar{J}_2 + (u_0-u_1)(u_0-u_2)\ln \bar{J}_3\right]$$

$$\bar{J}_i = \bar{J}(u_i)$$

and $\delta_g$ is the lethargy width of that portion of fine group g which is in the unresolved range.

## 2.4 EPITHERMAL SPECTRUM CALCULATION

The method used for computing the epithermal spectrum is the homogeneous $B_1$ method used in the code HRG3. The derivation which is presented here is adapted from the HRG3 manual (Reference 2-14).

The steady-state Boltzmann transport equation can be written as

$$\underline{\Omega}\cdot\nabla f(\underline{r},E,\underline{\Omega}) + \Sigma_t(\underline{r},E)f(\underline{r},E,\underline{\Omega})$$

$$= \int \Sigma_s(\underline{r},E'\rightarrow E,\underline{\Omega}'\rightarrow\underline{\Omega})f(\underline{r},E',\underline{\Omega}')dE'd\underline{\Omega}' + \frac{S(\underline{r},E)}{4\pi} \qquad (2\text{-}43)$$

where $f(\underline{r},E,\underline{\Omega})$ is the angular flux and the source is assumed to be isotropic.

To determine the energy dependence of the angular flux, the spatial dependence of Equation (2-43) must be removed. The spatial dependence appears explicitly only in the leakage term. Since leakage of epithermal neutrons is weakly dependent on the reactor's geometry, slab geometry can be used to approximate the first term of the transport equation. Representing the spatial variable by z, Equation (2-43) becomes

$$\mu \frac{\partial}{\partial z} f(z,E,\underline{\Omega}) + \Sigma_t(z,E)f(z,E,\underline{\Omega})$$

$$= \int \Sigma_s(z,E'\rightarrow E,\underline{\Omega}'\rightarrow\underline{\Omega})f(z,E',\underline{\Omega})dE'd\underline{\Omega}' + \frac{1}{4\pi} S(z,E) \qquad (2\text{-}44)$$

Now introduce the Legendre polynominal expansions for the flux and the scattering kernel:

$$f(z,E,\underline{\Omega}) = \sum_{\ell=0}^{\infty} \frac{2\ell+1}{4\pi} \Psi_\ell(z,E)P_\ell(\mu) \qquad (2\text{-}45)$$

$$\Sigma_s(z,E'\rightarrow E,\underline{\Omega}'\rightarrow\underline{\Omega}) = \sum_{\ell=0}^{\infty} \frac{2\ell+1}{4\pi} \Sigma_{s\ell}(z,E'\rightarrow E)P_\ell(\mu_L) \qquad (2\text{-}46)$$

where $\mu$ is the cosine of the angle between $\underline{\Omega}$ and the z axis and $\mu_L = \underline{\Omega}' \cdot \underline{\Omega}$ is the cosine of the scattering angle in laboratory coordinates. Substituting these expansions in Equation (2-44) yields

$$\sum_{\ell=0}^{\infty} \frac{2\ell+1}{4\pi} P_\ell(\mu) \left[ \mu \frac{\partial}{\partial z} \psi_\ell (z,E) + \Sigma_t(z,E)\psi_\ell(z,E) \right]$$

$$= \sum_{\ell=0}^{\infty} \frac{2\ell+1}{4\pi} P_\ell(\mu) \left[ \int \Sigma_{s\ell}(z,E' \rightarrow E)\psi_\ell(z,E')dE' + S(z,E)\delta_{\ell 0} \right] \quad (2\text{-}47)$$

where $\delta_{\ell 0}$ is a Kronecker delta equal to one when $\ell = 0$ and equal to zero otherwise. The Fourier transform is now taken:

$$\sum_{\ell=0}^{\infty} \frac{2\ell+1}{4\pi} P_\ell(\mu) \left[ -ik\mu \, \bar{\psi}_\ell(k,E) + \Sigma_{t\ell}(k,E) \, \bar{\psi}_\ell(k,E) \right]$$

$$= \sum_{\ell=0}^{\infty} \frac{2\ell+1}{4\pi} P_\ell(\mu) \left[ \int \Sigma_{s\ell}(k,E' \rightarrow E)\bar{\psi}_\ell(k,E')dE' + \bar{S}(k,E)\delta_{\ell 0} \right] \quad (2\text{-}48)$$

where

$$\bar{\psi}_\ell(k,E) = \int_{-\infty}^{\infty} e^{ikz} \psi_\ell(z,E)dz$$

and

$$\bar{S}(k,E) = \int_{-\infty}^{\infty} e^{ikz} S(z,E)dz$$

Note that k is equal to B, the square root of the geometric buckling. Also, we have assumed that the cross sections are independent of z and that the flux approaches zero as z approaches plus or minus infinity.

Equation (2-48) is now multiplied by

$$\frac{\Sigma_t(E)P_m(\mu)}{\Sigma_t(E)-ik\mu}$$

and integrated over all $\mu$, obtaining

$$\Sigma_t(E)\psi_m(k,E) = \sum_{\ell=0}^{\infty} (2\ell+1)A_{\ell m}(\upsilon)\left[\int \Sigma_{s\ell}(E'\rightarrow E)\psi_\ell(k,E')dE' + \bar{S}(k,E)\delta_{\ell 0}\right]$$

$$m = 0,1, \ldots\ldots \qquad (2\text{-}49)$$

where

$$\upsilon = \frac{\Sigma_t(E)}{ik}$$

and

$$A_{\ell m}(\upsilon) = \frac{\upsilon}{2}\int_{-1}^{1} \frac{P_\ell(\mu)P_m(\mu)}{\upsilon-\mu}\, d\mu \qquad (2\text{-}50)$$

$$= \upsilon\, P_j(\upsilon)\, Q_n(\upsilon) \qquad j = \min(\ell,m) \qquad n = \max(\ell,m)$$

The nth order Legendre functions of the second kind $Q_n(\upsilon)$ are defined

$$Q_0(\upsilon) = \frac{1}{2}\ln\left(\frac{\upsilon+1}{\upsilon-1}\right) \qquad Q_1(\upsilon) = \frac{1}{2}\upsilon\ln\left(\frac{\upsilon+1}{\upsilon-1}\right) - 1$$

The $B_1$ equations are obtained from Equation (2-49) by assuming that $\Sigma_{s\ell}(E'\rightarrow E) = 0$ for $\ell > 1$. After some simplifications the following equations are obtained:

$$kJ(E) + \Sigma_t(E)\phi(E) = \int \Sigma_{s0}(E'\rightarrow E)\phi(E')dE' + S(E) \qquad (2\text{-}51)$$

$$-\frac{1}{3}k\phi(E) + \alpha(E)\Sigma_t(E)J(E) = \int \Sigma_{s1}(E'\rightarrow E)J(E')dE' \qquad (2\text{-}52)$$

where

$$\alpha(E) = \frac{-A_{00}(\upsilon)}{3\upsilon^2\left[1-A_{00}(\upsilon)\right]} \qquad (2\text{-}53)$$

$$\phi(E) = \bar{\psi}_0(k,E) \tag{2-54}$$

$$J(E) = i\bar{\psi}_1(k,E) \tag{2-55}$$

$$S(E) = \bar{S}(k,E) \tag{2-56}$$

Integrating Equations (2-51) and (2-52) over each fine energy group results in the multigroup equations

$$kJ_g + \Sigma_{t,g}\phi_g = \sum_{g' \leq g} \Sigma_{s0}(E_{g'} \rightarrow E_g)\phi_{g'} + S_g \tag{2-57}$$

$$-\frac{1}{3} k\phi_g + \alpha_g \Sigma_{t,g} J_g = \sum_{g' \leq g} \Sigma_{s1}(E_{g'} \rightarrow E_g) J_{g'} \tag{2-58}$$

where

$$\phi_g = \int_{E_g}^{E_{g-1}} \phi(E)dE \tag{2-59}$$

$$J_g = \int_{E_g}^{E_{g-1}} J(E)dE \tag{2-60}$$

$$S_g = \int_{E_g}^{E_{g-1}} S(E)dE \tag{2-61}$$

$$\Sigma_{t,g} = \frac{1}{\phi_g} \int_{E_g}^{E_{g-1}} \Sigma_t(E)\phi(E)dE \tag{2-62}$$

Additional assumptions made were that the possible differences in $\Sigma_{t,g}$ due to its different energy weightings in Equations (2-57) and (2-58) could be neglected, $\Sigma_{s1}(E' \rightarrow E)$ could be flux weighted rather than current weighted, and that $\alpha_g$ can be evaluated from the fine group equivalent of Equation (2-53).

Equations (2-57) and (2-58) are applied to the homogenized assembly, hence the name "homogenized $B_1$ method". The cross sections required to solve the equations are averaged over a Cranberg fission spectrum with a 1/E tail for the fine groups in the fast energy range. In the resonance range, contributions to the fine group cross sections are calculated and averaged as described in the previous section. A factor dependent on the assembly hydrogen-to-heavy metal ratio (H/M) is used to reduce the lumped fission product epithermal cross sections calculated by CINDER, Section 2.7, to account for resonance shielding effects (Reference 2-15). A second factor, obtained from Monte Carlo studies, accounts for enhanced fast fission of U-238 due to heterogeneity effects in the lattice, and is also a function of H/M. The flux spectrum $\phi_g$ can now be calculated by solving Equations (2-57) and (2-58) simultaneously beginning with the highest energy group. Broad group parameters are obtained by averaging fine group values over the calculated spectrum for use in the CINDER fission product treatment and the assembly two-dimensional diffusion theory calculation.

## 2.5 THERMAL SPECTRUM CALCULATION

The thermal spectrum is obtained by using a nodal integral transport method (Reference 2-16) to solve the one-dimensional steady-state multigroup integral transport equation. This method is used with isotropic scattering in a heterogeneous system in cylindrical geometry. The method consists of constructing a set of coupled equations for neutron currents in terms of local escape and transmission probabilities and first-collision sources.

### 2.5.1 Theory

The steady-state, energy-dependent integral transport equation in the coordinate system shown in Figure 2-3 can be written as

$$\phi(\underline{r},E,\underline{\Omega}) = \int d\underline{r}' \; K(\underline{r}'\rightarrow\underline{r},E,\underline{\Omega})[H(\underline{r}',E,\underline{\Omega}) + S(\underline{r}',E,\underline{\Omega})] \qquad (2\text{-}63)$$

where

$\phi(\underline{r},E,\underline{\Omega})$ = the angular neutron flux,

$K(\underline{r}'\rightarrow\underline{r},E,\underline{\Omega})$ = the first-flight transport kernel,

$S(\underline{r}',E,\underline{\Omega})$ = any external source, and

$H(\underline{r}',E,\underline{\Omega})$ = the neutron emission density

$$= \int_{4\pi} d\underline{\Omega}' \int_0^\infty dE' \; \Sigma_s(\underline{r}',E'\rightarrow E,\underline{\Omega}'\rightarrow\underline{\Omega}) \; \phi(\underline{r}',E',\underline{\Omega}')$$

$$+ \frac{1}{\lambda} \int_{4\pi} d\underline{\Omega}' \int_0^\infty dE' \; \upsilon\Sigma_f(\underline{r}',E',\underline{\Omega}') \; \chi(\underline{r}',E'\rightarrow E,\underline{\Omega}'\rightarrow\underline{\Omega})$$

$$\cdot \; \phi(\underline{r}',E',\underline{\Omega}') \qquad (2\text{-}64)$$

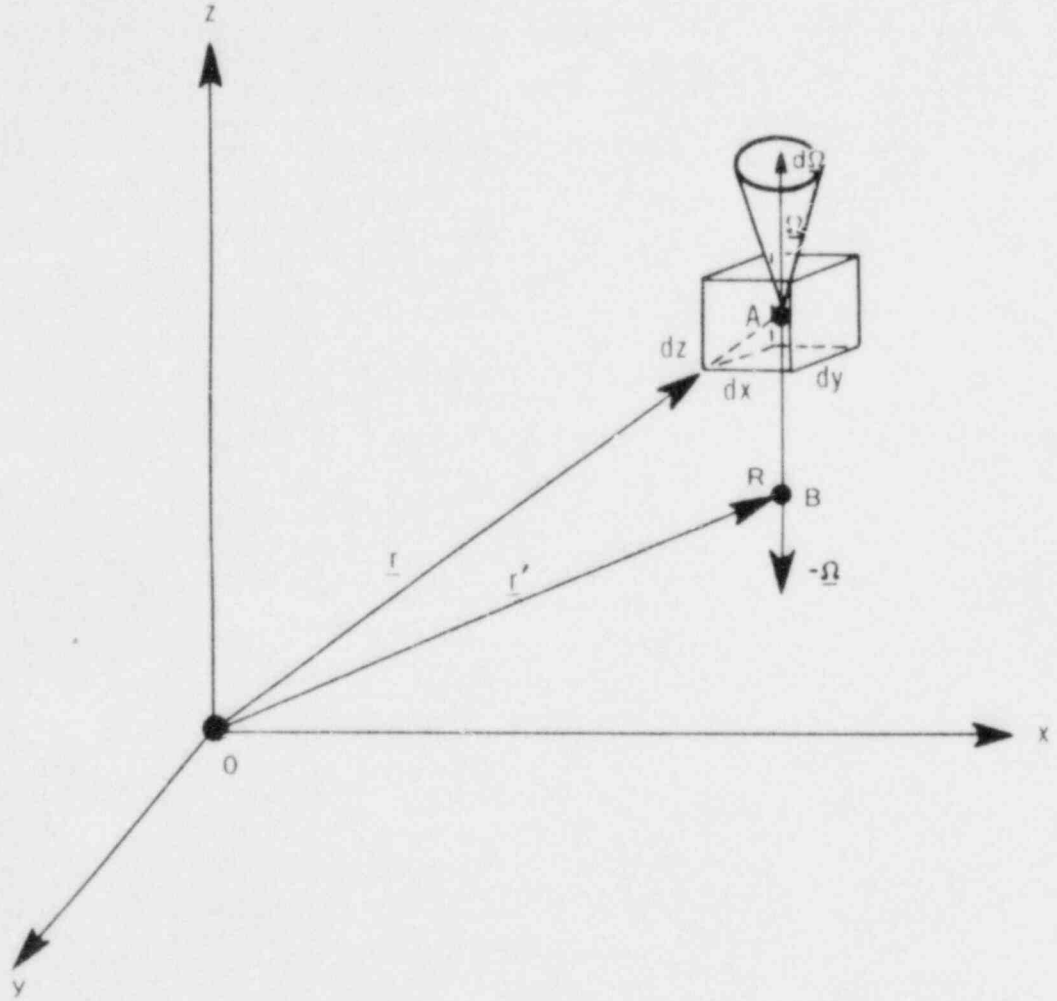


FIGURE 2-3: COORDINATES FOR THE INTEGRAL TRANSPORT EQUATION

where

$\Sigma_s$ = the scattering kernel,

$\chi$ = the fission spectrum, and

$\lambda$ = the eigenvalue of the system.

The nodal integral transport method transforms the conventional integral transport equation into an equivalent neutron current equation. The partial current at position $\underline{r}$ is defined as

$$J(\underline{r},E,\Delta\underline{\Omega}) = \int_{\Delta\underline{\Omega}} d\underline{\Omega}\ \underline{\Omega}\ \phi(\underline{r},E,\underline{\Omega}) \tag{2-65}$$

Substituting Equation (2-63) for the flux and defining the first collison source as

$$Q(\underline{r}',E,\underline{\Omega}) = H(\underline{r}',E,\underline{\Omega}) + S(\underline{r}',E,\underline{\Omega}) \tag{2-66}$$

yields

$$J(\underline{r},E,\Delta\underline{\Omega}) = \int d\underline{r}' \int_{\Delta\underline{\Omega}} d\underline{\Omega}\ \underline{\Omega}\ K(\underline{r}'\rightarrow\underline{r},E,\underline{\Omega})Q(\underline{r}',E,\underline{\Omega}) \tag{2-67}$$

The integral over space is divided into two parts: an integral over the local region of interest and another over the neighboring regions. Define the local escape probability,

$$P(\underline{r},E,\Delta\underline{\Omega}) = \frac{\int_{local} d\underline{r}' \int_{\Delta\underline{\Omega}} d\underline{\Omega}\ \underline{\Omega}\ K(\underline{r}'\rightarrow\underline{r},E,\underline{\Omega})Q(\underline{r}',E,\underline{\Omega})}{\int_{local} d\underline{r}' \int_{4\pi} d\underline{\Omega}\ \underline{\Omega}\ Q(\underline{r}',E,\underline{\Omega})}$$

the local average volume source,

$$\bar{Q}(E) = \frac{\int_{local} d\underline{r}' \int_{4\pi} d\underline{\Omega}\ Q(\underline{r}',E,\underline{\Omega})}{\int_{local} d\underline{r}' \int_{4\pi} d\underline{\Omega}}$$

the local transmission probability from neighbor n,

$$T_n(\underline{r},E,\Delta\underline{\Omega}) = \frac{\int_n d\underline{r}' \int_{\Delta\underline{\Omega}} d\underline{\Omega}\ \underline{\Omega}\ K(\underline{r}'\rightarrow\underline{r},E,\underline{\Omega})Q(\underline{r}',E,\underline{\Omega})}{\int_n d\underline{r}' \int_{4\pi} d\underline{\Omega}\ \underline{\Omega}\ Q(\underline{r}',E,\underline{\Omega})}$$

and the partial current of neighbor n:

$$J_n(\Sigma) = \int_n d\underline{r}' \int_{4\pi} d\underline{\Omega}\ \underline{\Omega}\ Q(\underline{r}',E,\underline{\Omega})$$

Then Equation (2-67) can be written as

$$J(\underline{r},E,\Delta\underline{\Omega}) = P(\underline{r},E,\Delta\underline{\Omega})\bar{Q}(E)\Delta V(\underline{r}) + \sum_{n=1}^{N} T_n(\underline{r},E,\Delta\underline{\Omega})\bar{J}_n(E) \qquad (2\text{-}68)$$

where $\Delta V(\underline{r})$ is the volume of the local region.

Equation (2-68) is the neutron balance equation, expressed in terms of partial currents and a volume source, applied to the local region at $\underline{r}$ under consideration. The calculation of the point-to-point transport kernel is now reduced to a calculation of a set of local escape and transmission probabilities, and the iterative solution of the fluxes is reduced to that of partial currents.

Once the converged set of partial currents is obtained, the neutron fluxes can be calculated using the law of neutron conservation applied to a given region of interest:

Collision rate = Volume source + Net entering current

$$\Sigma_t(\underline{r},E)\phi(\underline{r},E)\Delta V(\underline{r}) = \bar{Q}(E)\Delta V(\underline{r}) + J_{in}(\underline{r},E) \qquad (2\text{-}69)$$

where the angular dependence has been removed by integration over all solid angles.

2.5.2 Method of Solution

Equations (2-64), (2-68), and (2-69) form the theoretical basis of the nodal integral transport approximation. They are solved numerically in a modified THERMOS (Reference 2-17) with the method of cosine currents. To be compatible with THERMOS, the energy variable has been changed to velocity. The velocity space is divided into I intervals of width $\Delta v_i$ and $\underline{r}$ space into K regions of volume $\Delta V_k$. Define

$$F_{ki} = \phi(\underline{r}_k, v_i)$$

$$S_{ki} = S(\underline{r}_k, v_i)$$

$$H_{ki} = H(\underline{r}_k, v_i)$$

$$Q_{ki} = Q(\underline{r}_k, v_i)$$

$$= H_{ki} + S_{ki}$$

A uniform and isotropic volume source $Q_{ki}$ is assumed for each region. Also, it is assumed that the scattering kernel and fission spectrum are known so that $H_{ki}$ can be calculated from Equation (2-64). The external source $S_{ki}$ is known, thus $Q_{ki}$ can be determined.

The currents $J(\underline{r},E)$ can be defined in cylindrical geometry as shown in Figure 2-4. Then Equation (2-68) can be approximated as

$$J^{+}_{ki} = P^{o}_{ki}\, Q_{ki}\, \Delta V_k + T^{io}_{ki}\, J^{+}_{k-1,i} + T^{oo}_{ki}\, J^{-}_{ki} \qquad (2\text{-}70)$$

$$J^{-}_{k-1,i} = P^{i}_{ki}\, Q_{ki}\, \Delta V_k + T^{oi}_{ki}\, J^{-}_{ki} \qquad (2\text{-}71)$$

where for region k and velocity $v_i$,

$P^{o}_{ki}$ = the fraction of the uniform volume source which escapes through the outer surface,

$P^{i}_{ki}$ = the fraction of the uniform volume source which escapes through the inner surface,

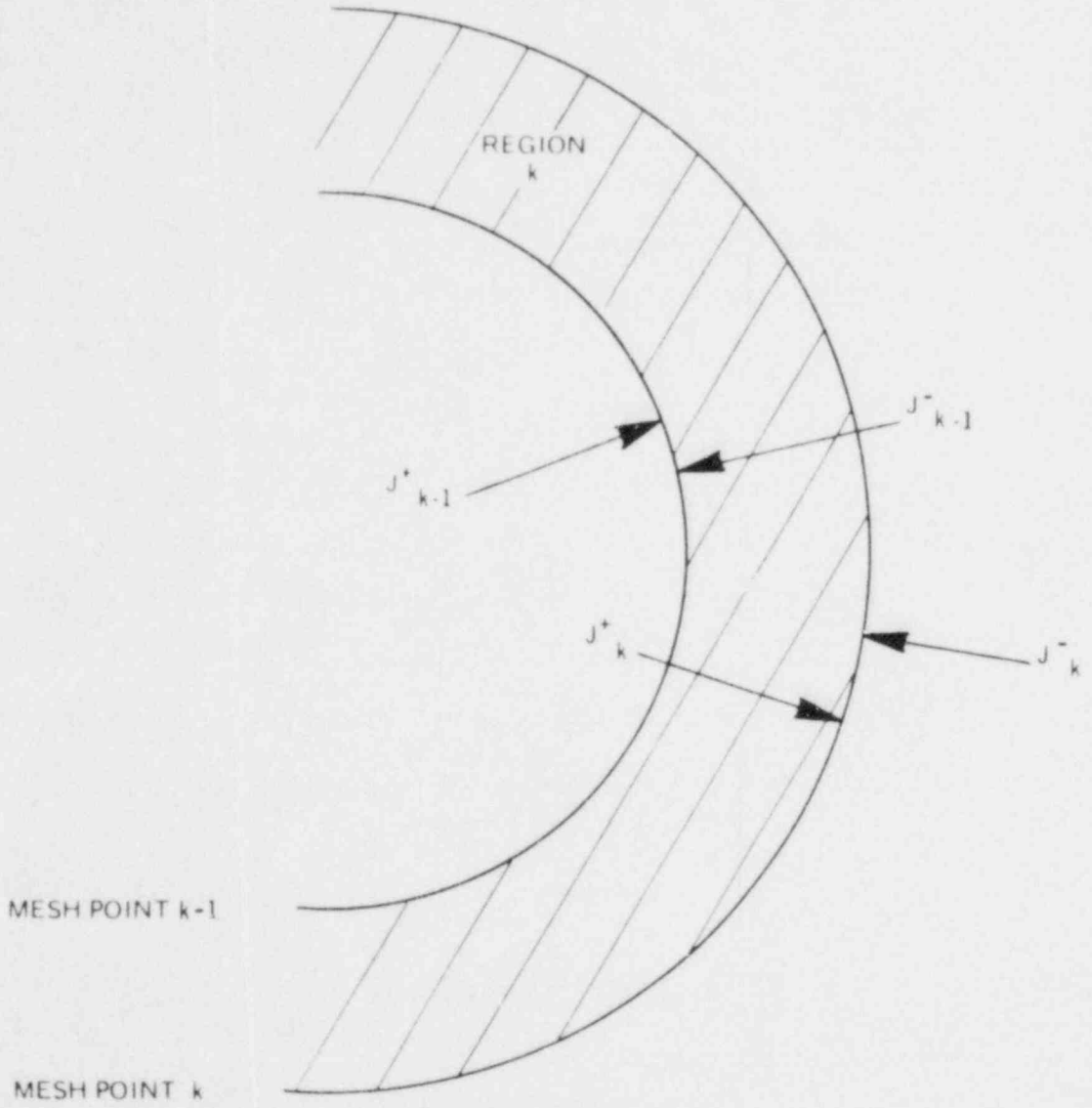


FIGURE 2-4: DEFINITION OF CURRENTS

$T^{io}_{ki}$ = the fraction of the cosine-shaped current on the inner surface which passes through the region and escapes through the outer surface,

$T^{oo}_{ki}$ = the fraction of the cosine-shaped current on the outer surface which passes through the region and escapes through the outer surface, and

$T^{oi}_{ki}$ = the fraction of a cosine-shaped current on the outer surface which passes through the region and escapes through the inner surface.

The above escape and transmission probabilities are interrelated:

$$T^{oi}_{ki} = \alpha_k \, T^{io}_{ki} \tag{2-72}$$

$$T^{io}_{ki} = 1 - \beta_{ki} \, P^{i}_{ki} \tag{2-73}$$

$$T^{oo}_{ki} = 1 - \alpha_k \left[ 1 + \beta_{ki} \, (P^{o}_{ki} - P^{i}_{ki}) \right] \tag{2-74}$$

with

$$\alpha_k = R_k / R_{k-1} \tag{2-75}$$

$$\beta_{ki} = 4 \, \Sigma_{ki} \, \Delta V_k / S_k \tag{2-76}$$

where

$\Sigma_{ki}$ = the total cross section of region k at velocity $v_i$,

$R_k$ = the outer radius of region k, and

$S_k$ = the outer surface area of region k.

Thus, only the escape probabilities $P^{o}_{ki}$ and $P^{i}_{ki}$ need to be calculated. As a result of the assumption of cosine currents, the escape probabilities are available from a correlation dependent on $\alpha_k$ and the region optical thickness.

The nodal flux is approximated from Equation (2-69) as:

$$F_{ki} = \frac{1}{\Sigma_k \Delta V_k} \left[ Q_{ki} \Delta V_k + (J^+_{k-1,i} - J^-_{k-1,i}) - (J^+_{ki} - J^-_{ki}) \right] \quad (2\text{-}77)$$

Since the volume source is a function of the flux, the above equation must be solved iteratively. Using an initial flux estimate, the volume source is calculated. The inward currents for each region are determined from Equation (2-71) beginning with the outermost region. Then the outward currents for each region are found using Equation (2-70) beginning from the innermost region. A zero net current boundary condition is satisfied by setting $J^+_{ki} = J^-_{ki}$ at the outer surface. The flux spectrum is determined using Equation (2-77) and the process repeated until convergence. The rate of convergence is improved using over-relaxation:

$$F^{j+1}_{ki} = F^j_{ki} + \delta(F^{j+1}_{ki} - F^j_{ki}) \quad (2\text{-}78)$$

where j is the iteration counter and $\delta$ is the over-relaxation parameter.

### 2.5.3 Geometry

In the spectrum calculations, the fuel pins are grouped according to their spectral environment. For a typical 8x8 BWR assembly, four fueled spectrum regions are used with a fifth spectrum region containing the channel and water gap surrounding the assembly (Figure 2-5). The flow area inside the channel not included in the unit cell areas defined by the lattice pitch is added to the moderator area associated with the outer ring of pins. Any water rods are included in spectrum region one.

Each fuel or poison pin and its surrounding clad and moderator is represented by a cylindrical unit cell of infinite length with the moderator radius chosen to conserve the total area of the cell (Figure 2-6). An average fuel cell is determined for each fueled spectrum region,

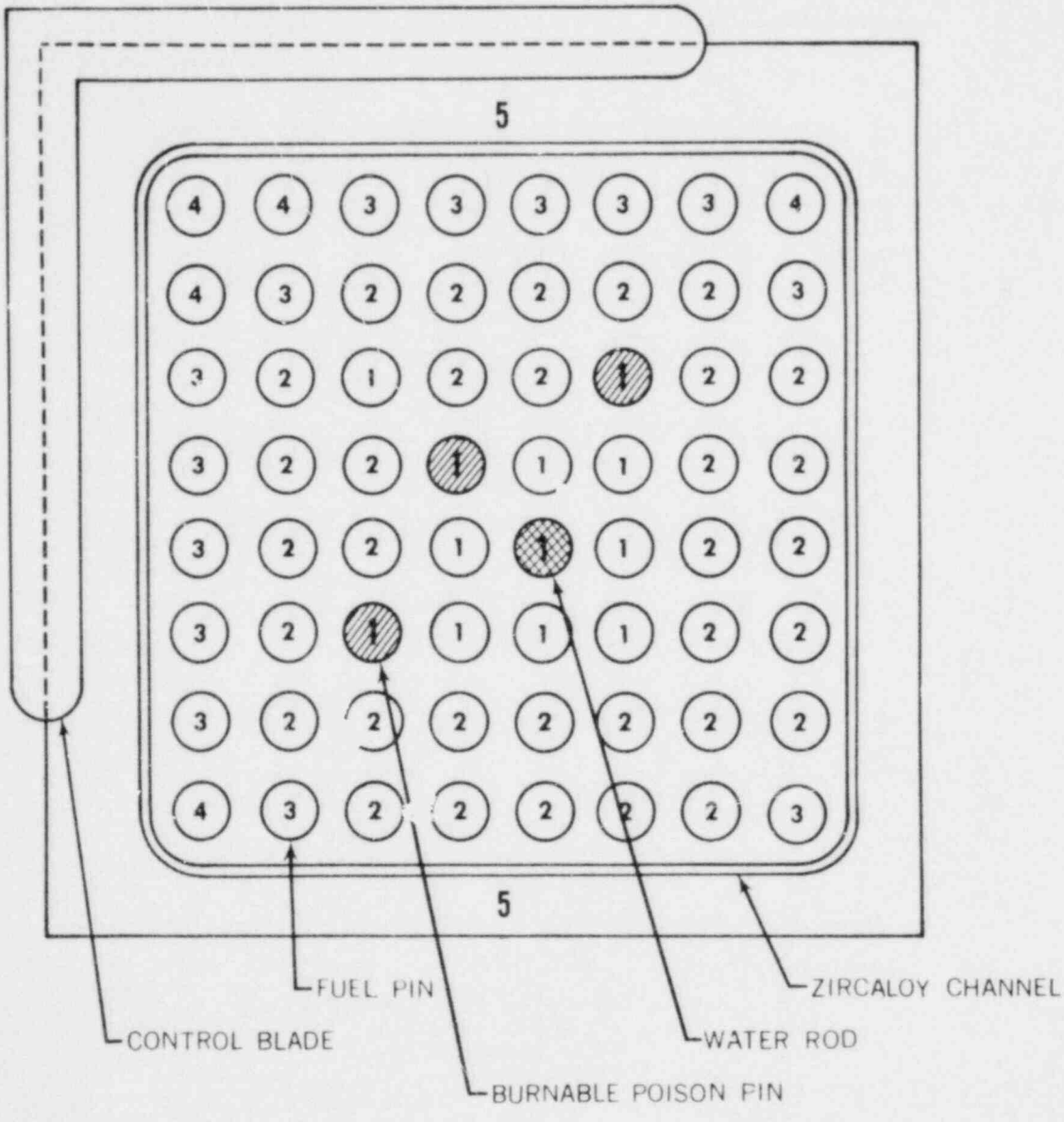


**FIGURE 2-5: BWR LATTICE CONFIGURATION**

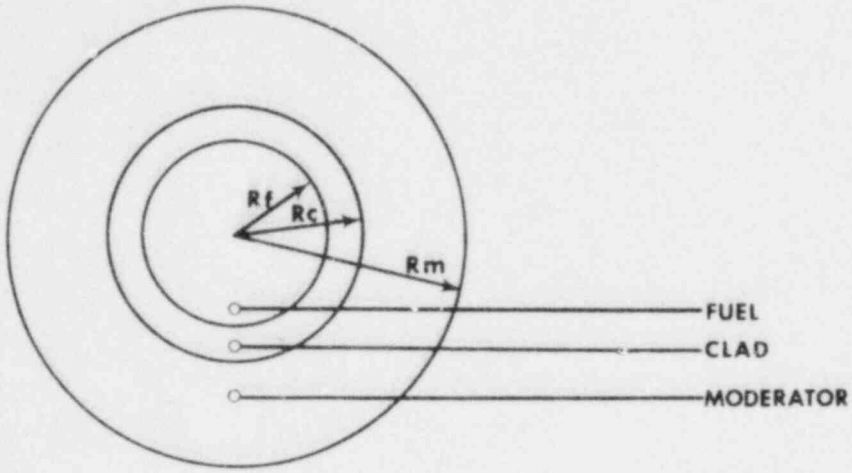


FIGURE 2-6: CYLINDRICIZED FUEL CELL

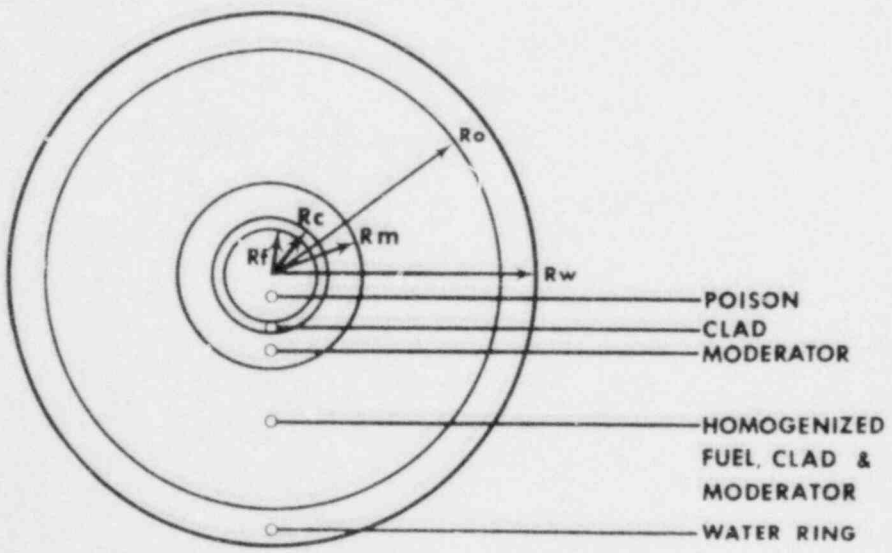


FIGURE 2-7: SUPER CELL MODEL

ignoring any poison cells, for which the spectrum will be calculated. This cell is typically divided into five rings in the fuel, a single ring in the clad, and six rings in the moderator. For poison cells, more spatial rings are included in the poison region, and a coupling region of homogenized fuel, clad, and moderator is added around the outside of the cell to create a super cell model of the poison cell and the surrounding lattice (Figure 2-7). The coupling region is needed to obtain the correct thermal spectrum in the poison pin; omission of the coupling region would represent an infinite array of poison cells. The composition and cross sections of the coupling region are obtained from the fuel cell calculation for the spectrum region in which the poison resides. The coupling region radius corresponds to five times the lattice cell pitch. Outside the coupling region, a water ring is added with the thickness chosen to match the average neutron velocity in the coupling region to that in the corresponding spectrum region obtained from the assembly spectrum calculation described below.

A space-dependent spectrum is determined using a one-dimensional cylindrical representation of the assembly to account for the interaction of spectrum regions. The assembly is divided into concentric rings, each corresponding to a spectrum region (Figure 2-8). The inner rings are the fueled spectrum regions ordered by spectrum region number with region one in the center. The outer ring corresponds to the homogenized channel and water gap and has a significant softening effect on the other spectrum regions. The ring thicknesses are chosen to conserve the volume fractions from the actual assembly configuration. Each ring is subdivided into several mesh intervals with the number proportional to its thickness.

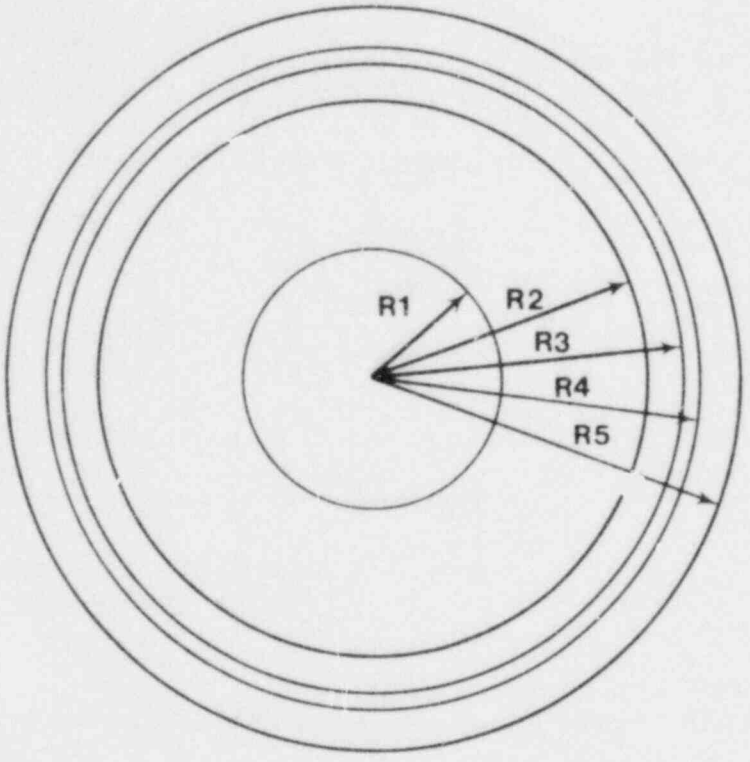


FIGURE 2-8: CYLINDRICIZED ASSEMBLY (8 x 8 BWR)

### 2.5.4 Thermal Cross Sections

Space dependent thermal spectrum calculations are made for the average fuel cell in each spectrum region. Effective microscopic cross sections in each energy group are determined by spatially averaging over the cell flux for use in the corresponding homogenized assembly region. For spectrum regions containing poison pins, the fuel cell cross sections are used in the coupling region of the super cell. The spectrum from the super cell calculation is used to average the cross sections in the super cell for the corresponding assembly region. Reaction rates from the fuel and super cells are conserved by modifying the assembly cross sections as follows.

For nuclide i, the cell reaction rate is

$$X_c^i(E) = \sigma_i(E)\int_c N_i(r)\phi(r,E)dr \qquad (2\text{-}79)$$

where the integral is over the cell volume,

$\sigma_i(E)$ = the THERMOS library cross section for nuclide i,

$N_i(r)$ = the concentration of nuclide i, and

$\phi(r,E)$ = the cell flux spectrum.

Expressing the nuclide concentration and the flux as volume averaged quantities, Equation (2-79) becomes

$$X_c^i(E) = \sigma_i(E)N_c^i\phi_c(E)V_c d_c^i(E) \qquad (2\text{-}80)$$

where

$$N_c^i = \frac{1}{V_c}\int_c N_i(r)dr$$

$$\phi_c(E) = \frac{1}{V_c}\int_c \phi(r,E)dr$$

$V_c$ = the volume of the lattice cell, and

$d_c^i(E)$ = the cell disadvantage factor for nuclide i

$$d_c^i(E) = \frac{\int_c N_i(r)\phi(r,E)dr}{N_c^i \phi_c(E) V_c}$$

Since nuclide reaction rates in the cell are conserved in the assembly region,

$$X_A^i(E) = X_c^i(E)$$

or

$$\sigma_A^i(E) N_A^i \phi_A(E) V_A = \sigma_i(E) d_c^i(E) N_c^i \phi_c(E) V_c \qquad (2\text{-}81)$$

where A denotes the assembly region. Thus the effective cross section for an assembly region is

$$\sigma_A^i(E) = \sigma_i(E) d_c^i(E) \frac{N_c^i \phi_c(E) V_c}{N_A^i \phi_A(E) V_A} \qquad (2\text{-}82)$$

Assuming that the flux integral is the same for the cell and the corresponding assembly region, Equation (2-82) becomes

$$\sigma_A{}^i(E) = \sigma_i(E) d_c^i(E) \frac{N_c^i}{N_A^i} \qquad (2\text{-}83)$$

or, in terms of non-averaged lattice cell parameters:

$$\sigma_A{}^i(E) = \sigma_i(E) \frac{\int_c N_i(r)\phi(r,E)dr}{N_A^i \int_c \phi(r,E)dr} \qquad (2\text{-}84)$$

The effective thermal cross sections determined from Equation (2-84) are used to calculate the thermal neutron spectrum in the assembly. Then the broad thermal group cross sections for the two-dimensional diffusion theory calculation can be found. The unit cells are modeled as homogenized regions in both the assembly spectrum calculation and optionally in the

diffusion theory calculation; hence, the broad group cross sections for each nuclide in the cell are the fine group cross sections for the corresponding assembly region averaged over the flux spectrum:

$$\sigma_i^{th} = \frac{\int_0^{E_{th}} \sigma_A{}^i(E)\phi_A(E)dE}{\int_0^{E_{th}} \phi_A(E)dE} \tag{2-85}$$

where $E_{th}$ is the thermal group cutoff energy.

Since diffusion theory significantly underestimates the flux depression in a highly absorbing rod, the poison cells are not homogenized in the two-dimensional diffusion theory calculation of the assembly. Each poison cell is modeled as a square poison region surrounded by its homogenized clad and moderator. This requires a procedure similar to that above to adjust the poison region cross sections to agree with the transport theory calculation. No correction is made to the clad-moderator cross sections. Therefore, a fixed source, one group, two-dimensional diffusion theory calculation is performed for a square representation of the super cell (Figure 2-9). Then the diffusion theory absorption cross section of the poison region is adjusted to conserve the fraction of absorptions in the poison region determined from the transport theory calculation for the super cell:

$$\frac{V_p \bar{\Sigma}^D_{a,p} \bar{\phi}^D_p}{V_c \bar{\Sigma}^D_{a,c} \bar{\phi}^D_c} = \frac{V_p \bar{\Sigma}^T_{a,p} \bar{\phi}^T_p}{V_c \bar{\Sigma}^T_{a,c} \bar{\phi}^T_c} \tag{2-86}$$

where

$V_R$ = the volume of region R,

$\bar{\Sigma}_{a,R}$ = the average macroscopic thermal absorption cross section of region R

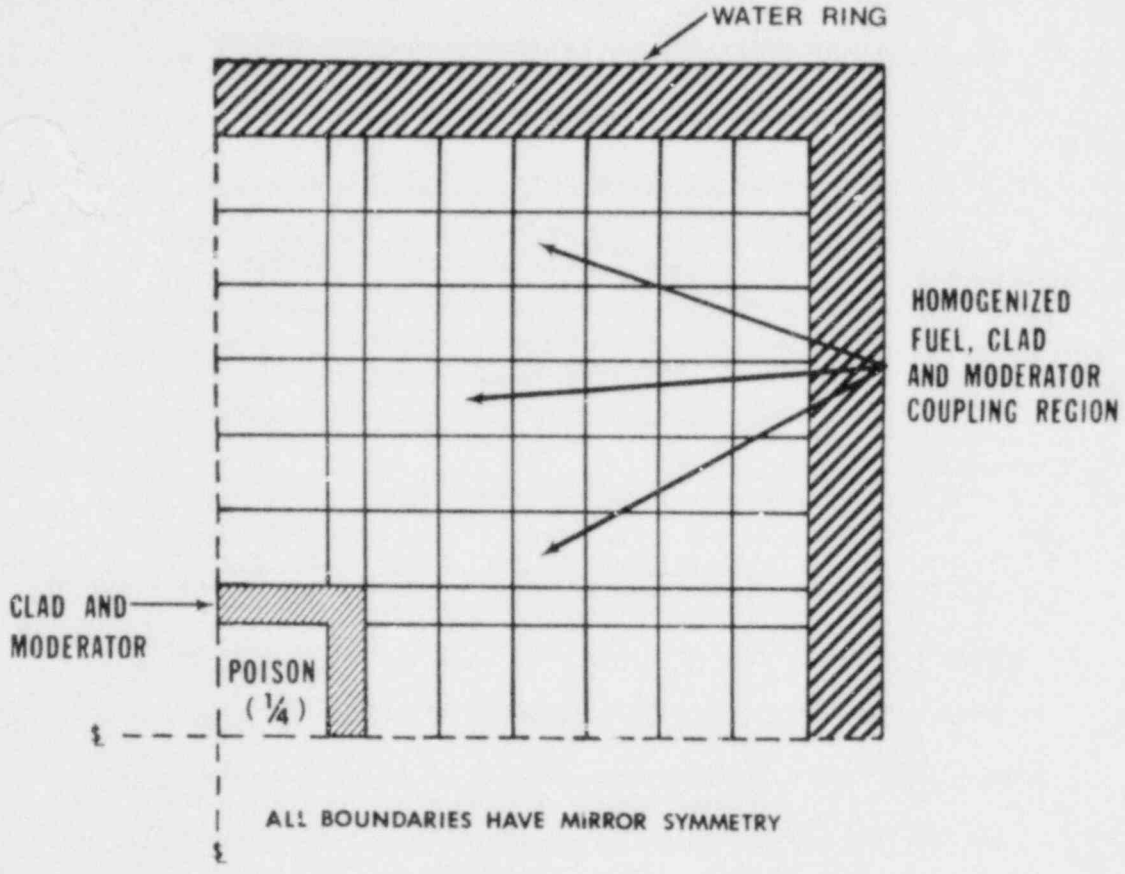


FIGURE 2-9: TWO-DIMENSIONAL MESH
FOR A SUPER CELL

$$\bar{\Sigma}_{a,R} = \frac{\sum_i \int_0^{E_{th}} \int_R N_i(r)\sigma_i(r,E)drdE}{\int_0^{E_{th}} dE \int_R dr}$$

$\bar{\phi}_R$ = the average thermal flux of region R

$$= \frac{\int_0^{E_{th}} \int_R \phi(r,E)drdE}{\int_0^{E_{th}} dE \int_R dr}$$

The subscript p refers to the poison region, c refers to the super cell, and the superscripts D and T refer to diffusion theory and transport theory results, respectively.

Solving for the diffusion theory absorption cross section in the poison region yields

$$\bar{\Sigma}^D_{a,p} = T_D \bar{\Sigma}^T_{a,p} \tag{2-87}$$

where

$$T_D = \frac{\bar{\Sigma}^D_{a,c}}{\bar{\Sigma}^T_{a,c}} \frac{\bar{\phi}^D_c}{\bar{\phi}^T_c} \frac{\bar{\phi}^T_p}{\bar{\phi}^D_p} \tag{2-88}$$

This correction is applied to all thermal cross sections for the poison region:

$$\sigma^{th}_{i,p} = T_D \sigma^{th}_i \tag{2-89}$$

where $\sigma^{th}_i$ is the cross section of the nuclide in the homogenized cell, given by Equation (2-85). Equations (2-87) and (2-88) must be solved iteratively because of the interaction of the diffusion theory cross sections and flux, but few iterations are required for convergence.

## 2.6 EFFECTIVE CONTROL ROD PARAMETERS

The effective few-group parameters for use in the control rod regions of the two-dimensional assembly calculations are determined using the code RODWORTH (Reference 2-18), modified by the Tennessee Valley Authority. Different methods are used to determine the effective few-group parameters depending upon the geometry of the control rods; for cruciform rods consisting of a linear array of cylindrical poison pins, the method devised by Michelini (Reference 2-19) is used, while the method of Sha (Reference 2-20) is used for rod cluster control (RCC) rods.

### 2.6.1 Control Blades

Michelini's method (Reference 2-19) combines $P_1$ blackness theory with geometrical considerations of the different paths that neutrons can take through a control blade filled with cylindrical poison pins. There are two possible paths of neutron penetration across the blade: through the slit due to the clad of the poison pins and through the poison itself (Figure 2-10). This differentiation allows the poison to be first considered black in order to calculate the transmission through the clad, then the additional transmission through the grey poison region can be evaluated.

First, it must be determined whether the poison is grey or black to neutrons in each energy group. To do this, the optical thickness $2\Sigma_a(R-a)$ of the poison region is estimated using fine group cross sections from a built-in library. If the optical thickness is greater than 7, the poison is considered black, and the transmission of the neutrons through the blade must be due entirely to the slit represented

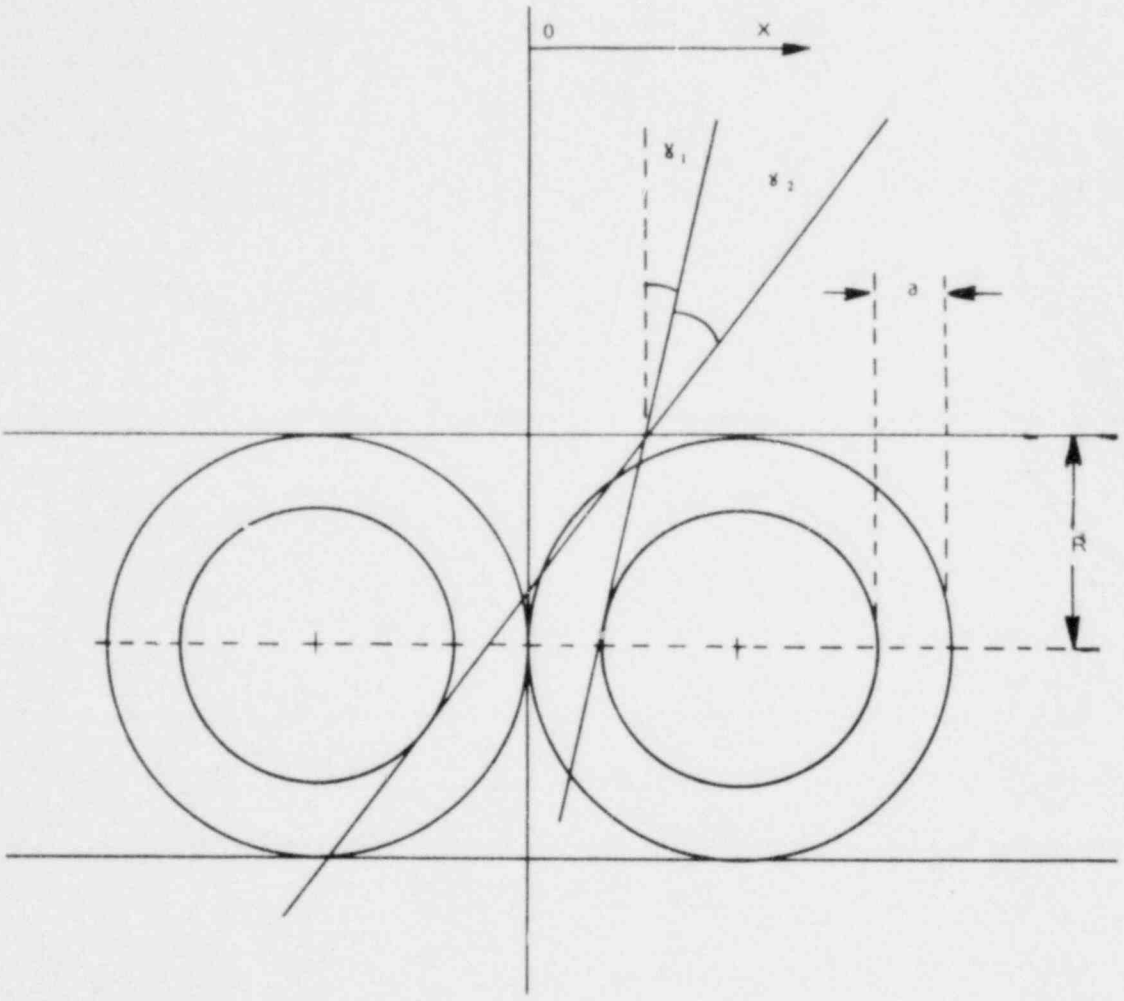


FIGURE 2-10: GEOMETRY OF POISON PINS IN A CONTROL BLADE

by the clad. Due to the small thickness of the clad, the probability that a neutron crossing the blade will undergo a collision in the clad is very small. Thus it is assumed that the fraction of the incoming neutrons which successfully cross the wall is, at any abscissa x, related to the angle $(\gamma_1 + \gamma_2)$ between the two trajectories tangential to the cylindrical poison regions (Figure 2-10). This angle is given by

$$\sin \gamma_1(x) = \frac{(R+x)\left[(R+x)^2 + 2aR - a^2\right]^{\frac{1}{2}} - R(R-a)}{(R+x)^2 + R^2} \tag{2-90}$$

$$\sin \gamma_2(x) = \frac{(R-x)\left[(R-x)^2 + 2aR - a^2\right]^{\frac{1}{2}} - R(R-a)}{(R-x)^2 + R^2} \tag{2-91}$$

where a is the thickness and R is the outer radius of the clad. Assuming a diffusive outside medium, the angular distribution of the incoming neutrons is

$$\Psi_i(\upsilon) = \frac{1}{4\pi}\left(\Phi_i + 3J_i \cos\upsilon\right) \tag{2-92}$$

where $J_i$ are the incoming net currents, $\Phi_i$ are the fluxes on the i = A,B opposite sides of the blade, and $\upsilon$ is the angle between the neutron trajectory and the normal to the blade surface.

If the $\theta$-axis is chosen parallel to the axis of the poison pin, the angular distribution becomes

$$\Psi_i(\theta,\phi) = \frac{1}{4\pi}\left(\Phi_i + 3J_i \sin\theta \cos\phi\right), \tag{2-93}$$

where the $\phi$-axis is normal to the interfaces between the pins.

Consider now the net currents entering the two sides at the point of abscissa x (Figure 2-10). The balance between the incoming and outgoing neutrons is, in spherical coordinates,

$$J_A(x) = \frac{1}{4}\Phi_A(x) + \frac{1}{2}J_A(x) - \frac{1}{4\pi}\bar{\Phi}_B\int_0^{\pi}\sin^2\theta\,d\theta\int_{-\gamma_2(x)}^{\gamma_1(x)}\cos\phi\,d\phi$$

(2-94)

$$- \frac{3}{4\pi}\bar{J}_B\int_0^{\pi}\sin^3\theta\,d\theta\int_{-\gamma_2(x)}^{\gamma_1(x)}\cos^2\phi\,d\phi$$

$$J_B(x) = \frac{1}{4}\Phi_B(x) + \frac{1}{2}J_B(x) - \frac{1}{4\pi}\bar{\Phi}_A\int_0^{\pi}\sin^2\theta\,d\theta\int_{-\gamma_2(x)}^{\gamma_1(x)}\cos\phi\,d\phi$$

(2-95)

$$- \frac{3}{4\pi}\bar{J}_A\int_0^{\pi}\sin^3\theta\,d\theta\int_{-\gamma_2(x)}^{\gamma_1(x)}\cos^2\phi\,d\phi$$

where $\bar{\Phi}_i$ and $\bar{J}_i$ $(i = A,B)$ are mean values along x.

Defining two transmission probabilities as

$$p_1(x) \equiv \frac{1}{2}\int_{-\gamma_2(x)}^{\gamma_1(x)}\cos\phi\,d\phi = \frac{1}{2}\left[\sin\gamma_1(x) + \sin\gamma_2(x)\right] \qquad (2\text{-}96)$$

$$p_2(x) \equiv \int_{-\gamma_2(x)}^{\nu_1(x)}\cos^2\phi\,d\phi = \frac{2}{\pi}\left[\frac{\gamma_1(x) + \gamma_2(x)}{2} + \frac{\sin2\gamma_1(x) + \sin2\gamma_2(x)}{4}\right]$$

(2-97)

then Equations (2-94) and (2-95) become

$$J_A(x) = \frac{1}{4}\phi_A(x) + \frac{1}{2}J_A(x) - \frac{1}{4}\bar{\phi}_B p_1(x) - \frac{1}{2}\bar{J}_B p_2(x) \qquad (2\text{-}98)$$

$$J_B(x) = \frac{1}{4}\phi_B(x) + \frac{1}{2}J_B(x) - \frac{1}{4}\bar{\phi}_A p_1(x) - \frac{1}{2}\bar{J}_A p_2(x) \qquad (2\text{-}99)$$

To clear Equations (2-98) and (2-99) of the spatial dependence, the mean values of the currents, fluxes, and the transmission probabilities are introduced:

$$\bar{p}_1 = \frac{1}{R}\int_0^{\Delta x} p_1(x)dx \quad , \quad \bar{p}_2 = \frac{1}{R}\int_0^{\Delta x} p_2(x)dx \tag{2-100}$$

where $\Delta x$ is the distance at which $p_1(x)$ and $p_2(x)$ vanish. Now combining Equations (2-98) and (2-99) yields the $P_1$ blackness theory parameters $\alpha$ and $\beta$:

$$\alpha \equiv \frac{\bar{J}_A + \bar{J}_B}{\bar{\Phi}_A + \bar{\Phi}_B} = \frac{1}{2}\frac{1 - \bar{p}_1}{1 + \bar{p}_2}$$

$$\beta \equiv \frac{\bar{J}_A - \bar{J}_B}{\bar{\Phi}_A - \bar{\Phi}_B} = \frac{1}{2}\frac{1 + \bar{p}_1}{1 - \bar{p}_2} \tag{2-101}$$

The expressions for $\bar{p}_1$ and $\bar{p}_2$ have been approximately evaluated as

$$\bar{p}_1 = \frac{p_{10} f_1 \Delta x}{R}$$

$$\bar{p}_2 = \frac{p_{20} f_2 \Delta x}{R} \tag{2-102}$$

The first factor in these formulas is the transmission probability evaluated from Equations (2-96) and (2-97) at the point $x = 0$ under the assumption that $\sin\gamma_i(0) \cong \gamma_i(0)$, i.e., $a/R << 1$:

$$p_{10} \cong \frac{a}{R}\left[1 - \frac{a}{2(R+a)}\right] \tag{2-103}$$

$$p_{20} \cong \frac{4}{\pi}\frac{a}{R}\left[1 - \frac{a}{2(R+a)}\right] \tag{2-104}$$

The second factor is an estimated shape factor of the function $p_i(x)$ in the interval $0 \leq x \leq \Delta x$,

$$f_i = \frac{1}{2} + \frac{0.167}{1+\omega_i a/R} \quad , \quad i = 1,2 \tag{2-105}$$

At the point $x = 0$ these functions have a maximum and then gradually decrease and reach zero at $\Delta x$. Michelini reports that the values for $\omega_1$ and $\omega_2$ are 2.33 and 3.70, respectively, for $a/R < 0.3$.

The last factor,

$$\Delta x = \frac{R[a(2R-a)]^{\frac{1}{2}}}{R-a} \qquad (2\text{-}106)$$

is, as defined for Equation (2-100), the distance at which $p_1(x) = p_2(x) = 0$ (the distance at which the slit is no longer seen by the neutrons), and is determined from Equations (2-90) and (2-91) by setting $\gamma_1(\Delta x) = -\gamma_2(\Delta x)$.

In practice, the validity of the assumption used in the evaluation of the first and second factors of Equation (2-102) is confirmed since the clad thickness is not large with respect to its outer radius. Thus, the transmission probabilities for the case of black poison in the pins are:

$$\bar{p}_i = K_i \left[1 - \frac{a}{2(R+a)}\right] \frac{a[a(2R-a)]^{\frac{1}{2}}}{R(R-a)} \left(\frac{1}{2} + \frac{0.167}{1+\omega_i a/R}\right), \quad i = 1,2 \qquad (2\text{-}107)$$

where

$$K_1 = 1 \qquad K_2 = 4/\pi$$

$$\omega_1 = 2.33 \qquad \omega_2 = 3.70$$

If the poison is grey, i.e., the optical thickness is less than 7, then a fraction of the neutrons which impinge upon the poison region is transmitted through the pin. If one sets $p_{black} = (\bar{p}_1 + \bar{p}_2)/2$, and normalize to one entering neutron, then $p_{black}$ represents the neutrons passing through the slits and the $(1-p_{black})$ remaining neutrons must have trajectories which cross the poison material. If $p_o$ represents the attenuation suffered by the neutrons crossing the poison, then the total transmission probability across a blade with grey poison in the pins is

$$p = p_{black} + (1 - p_{black})\, p_o \qquad (2\text{-}108)$$

Since neutrons may pass through more than one poison region, the calculation of $p_o$ is a formidable task. Therefore, $p_o$ is approximately evaluated based on the fact that the probability $p_o(x)$, i.e., the

ttenuation suffered at any point, does not vary significantly along x. To explain this fact consider the neutrons crossing the poison material as being of one of two groups: those which cross only one poison region and those which cross more than one.

The first group of neutrons cross only one cylindrical poison region with the cylinder seen at different angles by the neutrons. Consider the mean attenuation suffered by the current of neutrons which crosses a poison region starting isotropically from a point on the x axis at the distance $[R^2 + (R+x)^2]^{\frac{1}{2}}$ from the pin axis (Figure 2-10):

$$\mu(x) = \frac{\int_0^{\pi} \sin^2\theta \, d\theta \int_{-\varepsilon}^{\varepsilon} \cos(\gamma+\phi) \exp[-\Sigma_a c(\theta,\phi)] d\phi}{\int_0^{\pi} \sin^2\theta \, d\theta \int_{-\varepsilon}^{\varepsilon} \cos(\gamma+\phi) \, d\phi} \qquad (2\text{-}109)$$

where

$$\varepsilon = \sin^{-1} \frac{R-a}{[R^2+(R+x)^2]^{\frac{1}{2}}} \quad , \quad \gamma = \sin^{-1} \frac{R+x}{[R^2+(R+x)^2]^{\frac{1}{2}}}$$

and

$$c(\theta,\phi) = \frac{2}{\sin\theta} \left\{ (R-a)^2 - [R^2+(R+x)^2] \sin^2\phi \right\}^{\frac{1}{2}} \qquad (2\text{-}110)$$

is the segment of trajectory within the poison.

Expanding the exponential up to the second derivative and performing the integrations results in the following expression which is valid for low absorbing materials ($\Sigma_a d \leq 0.3$):

$$\mu = 1-\Sigma_a d + 2/3 \, (\Sigma_a d)^2 \qquad (2\text{-}111)$$

where $d = 2(R-a)$ is the diameter of the poison region. Note that Equation (2-111) does not show any dependence on x. Thus, the mean attenuation $\mu$ remains unchanged within the poison, neglecting the high-order derivative effects not appearing in Equation (2-111).

The second group of neutrons suffers an attenuation $\mu_n$ which produces a small decrease in the total attenuation $p_o$. Since the sum of the path lengths within the various poison regions is about the same for any given trajectory, $\mu_n$ is practically the same at any point in the poison. Numerical estimations of $\mu_n$ and related averages on the populations of the two neutron groups gives consistently for a wide range of a/R ratios

$$p_o \cong \mu\ [0.84 + 0.16\ \exp(-0.6\Sigma_a d)] \tag{2-112}$$

which is valid under the same restrictions as Equation (2-111).

Since the restriction on $\mu$ is due only to the truncation of the power expansion, one suspects that a more general law exists whose power expansion approaches Equation (2-111). The following expression has been found valid in general:

$$p_o \cong \exp(-\Sigma_a d)[0.84 + 0.16\ \exp(-0.6\Sigma_a d)] \tag{2-113}$$

It should be noted that owing to the uncertainties of the spectral averages and to the approximations needed in the derivation of $p_o$, the differentiation of the transmission probability into two components, $p_1$ and $p_2$, loses its significance. Hence, the standard blackness parameters reduce to

$$\alpha = \frac{1}{2}\frac{1 - p}{1 + p}$$
$$\beta = \frac{1}{2}\frac{1 + p}{1 - p} \tag{2-114}$$

where p is given by Equation (2-108).

The group average blackness parameters are obtained by weighting $\alpha(E)$ and $\beta(E)$ by the flux spectrum. For the single thermal broad group, the flux spectrum is chosen such that the average parameters yield the same absorption rate obtained from the multigroup calculation. The spectrum required is the asymptotic flux in the medium surrounding the

control rod (Reference 2-21). This is the same as the flux spectrum in the region with the control rod withdrawn, which is calculated by LATTICE for input to RODWORTH. Thus, for the thermal group,

$$\bar{\alpha}_{th} = \frac{\int_0^{E_{th}} \alpha(E)\phi_\infty(E)dE}{\int_0^{E_{th}} \phi_\infty(E)dE}$$

$$\bar{\beta}_{th} = \frac{\int_0^{E_{th}} \beta(E)\phi_\infty(E)dE}{\int_0^{E_{th}} \phi_\infty(E)dE} \qquad (2\text{-}115)$$

where $E_{th}$ = 1.855 eV is the cutoff energy of the thermal group.

In the epithermal energy ranges, the flux spectrum used for averaging is that at the control rod surface (Reference 2-21):

$$\bar{\alpha}_g = \frac{\int_{E_g}^{E_{g+1}} \alpha(E)\ \phi(E,R)dE}{\int_{E_g}^{E_{g+1}} \phi(E,R)dE}$$

$$\bar{\beta}_g = \frac{\int_{E_g}^{E_{g+1}} \beta(E)\ \phi(E,R)dE}{\int_{E_g}^{E_{g+1}} \phi(E,R)dE} \qquad (2\text{-}116)$$

where $E_g$ is the lower energy limit of broad group g, and R denotes the control rod surface (Figure 2-10). Diffusion theory is used to determine

the flux distribution in the region external to the control rod, assuming a uniform spatial source distribution (Reference 2-21). The flux distribution is evaluated at the control rod surface and substituted into Equation (2-116) to determine the average blackness parameters.

The diffusion equation for any energy group in the region around the control rod is

$$D(E)\nabla^2\phi(E,x) - \Sigma_a(E)\phi(E,x) + S(E) = 0 \qquad (2\text{-}117)$$

with the boundary conditions

$$\nabla\phi = 0 \quad \text{at} \quad x = H$$

$$\frac{D\nabla\phi}{\phi} = \alpha \quad \text{at} \quad x = R$$

where H is the distance to the external region boundary. Note that for nonthermal energy groups, $\Sigma_a$ includes both absorption and removal from the group due to scattering.

For a control blade, Equation (2-117) yields

$$\phi(E,x) = \frac{S}{\Sigma_a}\left[\frac{1 + \frac{\alpha}{D\kappa}\,\frac{\lambda_1(x) - \lambda_1(R)}{\lambda_2(R)}}{1 - \frac{\alpha}{D\kappa}\,\frac{\lambda_1(R)}{\lambda_2(R)}}\right] \qquad (2\text{-}118)$$

where

$$\kappa^2 = \Sigma_a/D$$

$$\lambda_1(x) = \sinh(\kappa x) - \coth(\kappa H)\cosh(\kappa x)$$

$$\lambda_2(x) = \cosh(\kappa x) - \coth(\kappa H)\sinh(\kappa x)$$

When evaluated at the control rod surface, Equation (2-118) becomes

$$\phi(E,R) = \frac{S}{\Sigma_a}\left[\frac{1}{1 - \frac{\alpha}{D\kappa}\,\frac{\lambda_1(R)}{\lambda_2(R)}}\right] \qquad (2\text{-}119)$$

For practical problems, $\kappa R$ is small and $\kappa H$ is large, so

$$\lambda_1(R) \cong - \coth(\kappa H) \cong - 1$$

$$\lambda_2(R) \cong 1$$

Also assuming that $\Sigma_a \cong \Sigma_{tr}$,

$$\frac{1}{D\kappa} = \sqrt{3\Sigma_a/\Sigma_{tr}} \cong \sqrt{3}$$

Substituting yields

$$\varphi(E,R) = \frac{S(E)}{\Sigma_a(E)} \left[ \frac{1}{1 + \sqrt{3}\ \alpha(E)} \right] \tag{2-120}$$

The factor in brackets accounts for the flux depression at the control rod surface relative to the asymptotic flux $S/\Sigma_a$. Equation (2-120) can be rewritten as

$$\phi(E,R) = \phi_\infty(E) \left[ \frac{1}{1 + \sqrt{3}\ \alpha(E)} \right] \tag{2-121}$$

where $\phi_\infty$ is the flux spectrum calculated by LATTICE and input to RODWORTH. Therefore, for the epithermal groups,

$$\bar{\alpha}_g = \frac{\displaystyle\int_{E_g}^{E_{g+1}} \frac{\alpha(E)\phi_\infty(E)dE}{1 + \sqrt{3}\ \alpha(E)}}{\displaystyle\int_{E_g}^{E_{g+1}} \frac{\phi_\infty(E)dE}{1 + \sqrt{3}\ \alpha(E)}} \tag{2-122}$$

A similar derivation using $\beta$ instead of $\alpha$ as the boundary condition at the rod surface for the diffusion equation yields

$$\bar{\beta}_g = \frac{\displaystyle\int_{E_g}^{E_{g+1}} \frac{\beta(E)\phi_\infty(E)dE}{1 + \sqrt{3}\ \beta(E)}}{\displaystyle\int_{E_g}^{E_{g+1}} \frac{\phi_\infty(E)dE}{1 + \sqrt{3}\ \beta(E)}} \tag{2-123}$$

The macroscopic absorption cross section and the diffusion coefficient of the blade for each energy group are calculated for zero and one internal mesh point by the equations:

a) Zero internal mesh points

$$\Sigma_a = 2\,\bar{\alpha}/h$$

$$D = \frac{h}{2}\,(\bar{\beta} - \bar{\alpha}) \qquad (2\text{-}124)$$

where h, the mesh thickness, is the diameter of the poison pins.

b) One internal mesh point

$$\Sigma_a = \frac{2}{h}\left[\bar{\beta} - \sqrt{\bar{\beta}(\bar{\beta} - \bar{\alpha})}\right]$$

$$D = h\,\sqrt{\bar{\beta}(\bar{\beta} - \bar{\alpha})} \qquad (2\text{-}125)$$

where h is the poison pin radius.

2.6.2 RCC Rods

Sha's method for determining the effective few group parameters for RCC rods (Reference 2-20) is based on applying the diffusion equation in the region exterior to the control rod subject to transport theory boundary conditions at the surface of the rod.

For cylindrical absorbing elements that are uniformly distributed throughout the core (or follow a definite pattern), the problem may be treated by considering a control rod cell as shown in Figure 2-11. The control rod with radius $R_0$ is located at the center of the cell and the lattice area associated with the control rod is replaced by the concentric annulus with radius $R_1$. In the following derivation the control rod is assumed to be infinitely long and thus the problem under consideration is reduced to one dimension.

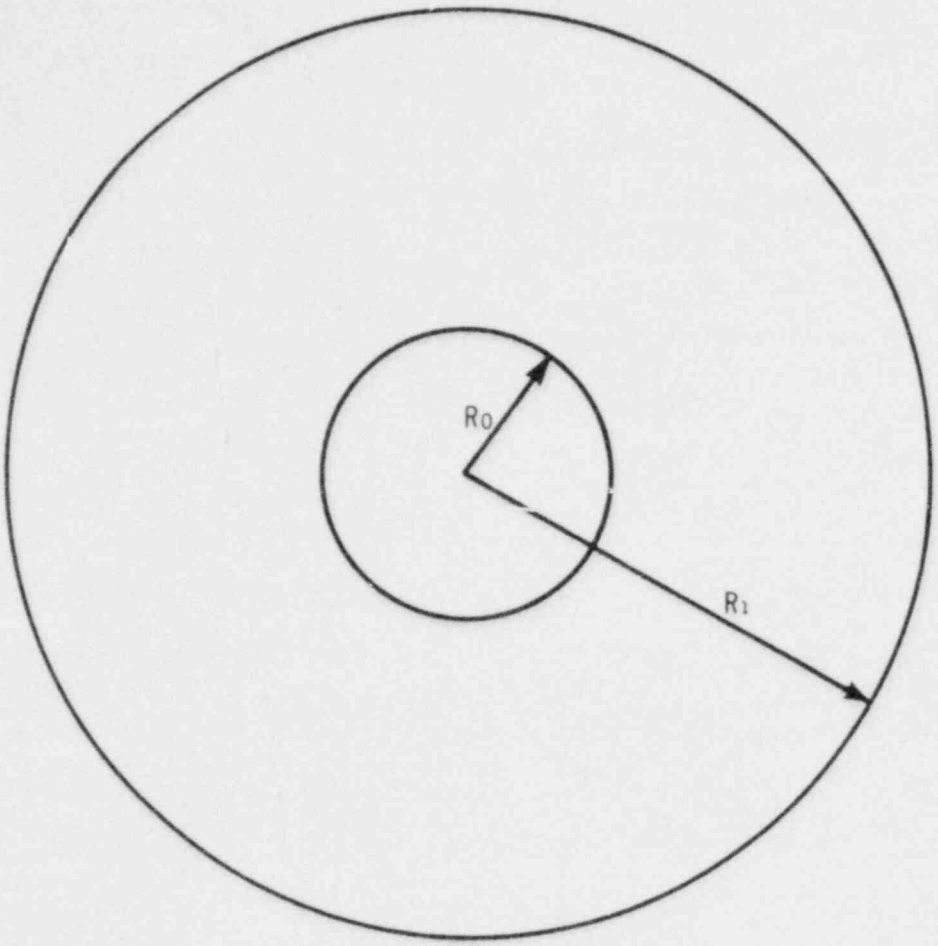


FIGURE 2-11: RCC ROD CELL

The neutron balance through the control rod surface is

$$J_{in}(E) - J_{out}(E) = \beta(E)\, J_{in}(E) \qquad (2\text{-}126)$$

where

$J_{in}(E)$ = the neutron current per unit surface area in the energy interval E to (E+dE) entering the surface of the control rod,

$J_{out}(E)$ = the neutron current per unit surface area in the energy interval E to (E+dE) leaving the surface of the control rod, and

$\beta(E)$ = the incident neutron capture probability for neutrons with energy E (blackness).

Assuming diffusion theory to be valid in the region external to the rod, the net current at the surface of the control rod is

$$D(E)\nabla\phi(E,R_0) = J_{in}(E) - J_{out}(E) = \beta(E)\, J_{in}(E) \qquad (2\text{-}127)$$

The entering current $J_{in}(E)$ can be expressed as

$$J_{in}(E) = \frac{1}{4}\,\phi(E,R_0) + \frac{1}{2}\,D(E)\nabla\phi(E,R_0) \qquad (2\text{-}128)$$

Substituting Equation (2-128) into Equation (2-127) yields

$$D(E)\nabla\phi(E,R_0) = \beta(E)\left[\frac{\phi(E,R_0)}{4} + \frac{D(E)}{2}\,\nabla\phi(E,R_0)\right]$$

Therefore, the ratio of neutron current to flux at the surface of the rod is

$$\alpha(E) \equiv \frac{D(E)\nabla\phi(E,R_0)}{\phi(E,R_0)} = \frac{\beta(E)}{2[2-\beta(E)]} \qquad (2\text{-}129)$$

In order to calculate $\alpha(E)$, the blackness of the control rod $\beta(E)$ must be evaluated. Blackness is a difficult quantity to calculate, and is a function of the control rod material, the size of the rod, and the neutron current distribution entering the surface of the rod.

However, $\beta$ has been calculated extensively (References 2-22 and 2-23) and is shown in Figure 2-12. The energy dependence of the blackness is implicit in the control rod cross sections used in reading the plot.

For the thermal energy range, represented by one broad group, Maxwellian averaged cross sections are used to determine $\beta$ since studies indicate that the use of hardened constants leads to poorer agreement between theoretical and experimental results. Therefore, only an average value for the blackness is obtained, and the thermal group current-to-flux ratio at the rod surface is calculated from Equation (2-129):

$$\bar{\alpha}_{th} = \frac{\bar{\beta}_{th}}{2(2-\bar{\beta}_{th})} \tag{2-130}$$

It should be pointed out that Equation (2-129) was derived based on cylindrical geometry and diffusion theory. However, these results will be used in the two-dimensional calculation of the assembly with square geometry and transport corrected cross sections. To account for these differences, Equation (2-130) is modified as follows:

$$\bar{\alpha}_{th} = \frac{\bar{\beta}_{th}}{2(2-\bar{\beta}_{th})} \; C_T \, C_S \tag{2-131}$$

The transport correction factor $C_T$ accounts for the effect of predicting the extrapolation distance with diffusion theory instead of transport theory. Since $\alpha$ is inversely proportional to the extrapolation distance,

$$C_T \equiv (\tfrac{2}{3} \lambda_{tr})/\delta \tag{2-132}$$

where $\delta$ is the transport theory extrapolation distance and $\lambda_{tr}$ is the transport mean free path of the medium surrounding the control rod. Figure 2-13 is a plot of $\delta/\lambda_{tr}$ as a function of $R_0/\lambda_{tr}$.

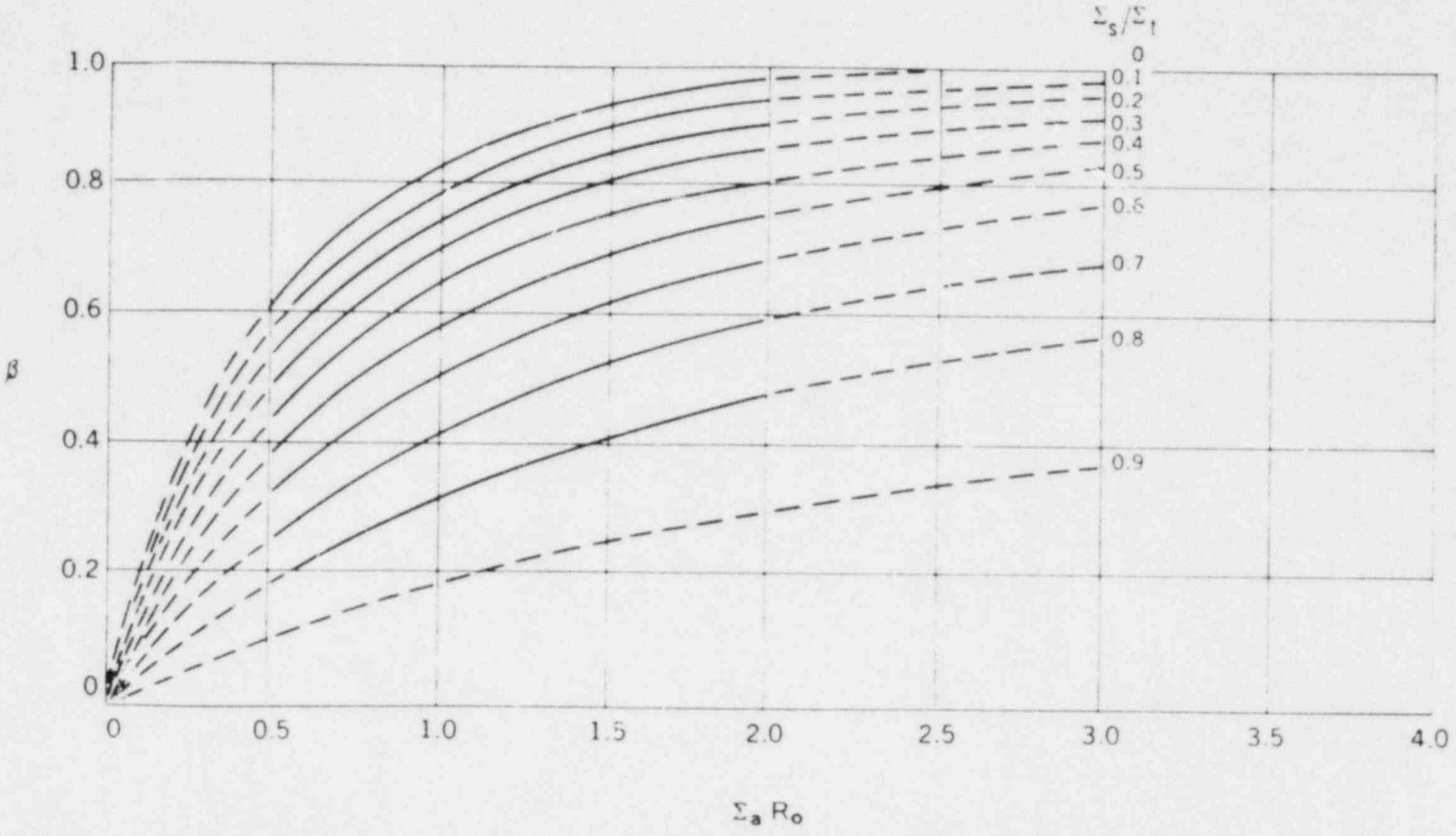


FIGURE 2-12: BLACKNESS OF CYLINDRICAL ABSORBERS

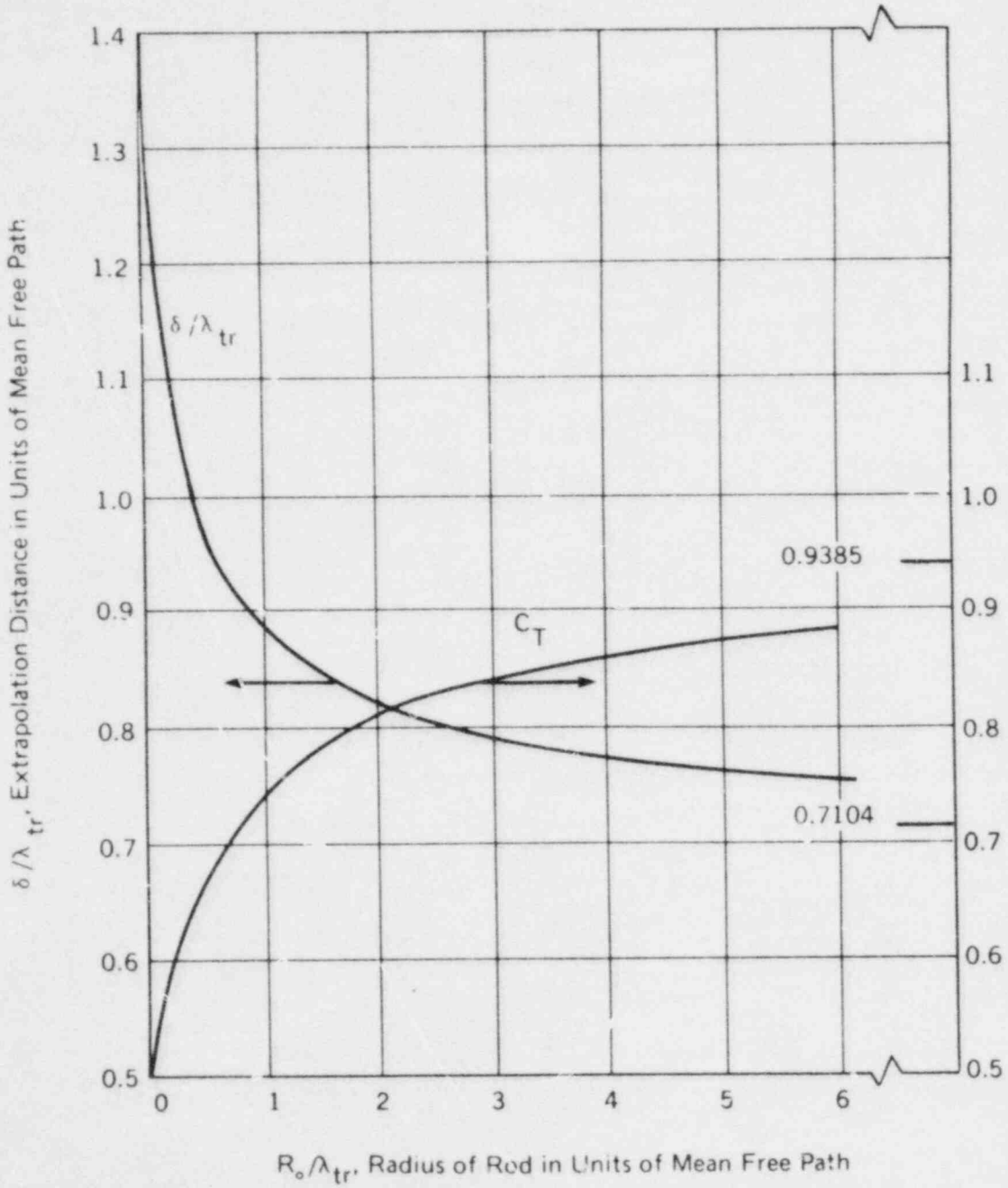


**FIGURE 2-13: TRANSPORT CORRECTION FACTOR FOR CYLINDRICAL ABSORBERS**

The factor $C_S$ is to correct for the change in leakage from cylindrical to square geometry. It is assumed that the leakage from the rod should be conserved and the neutron current would remain constant after the transformation of geometry. Therefore, $C_S$ is the ratio of the actual rod surface area to the surface area of a square rod

$$C_S = \frac{2\pi R_0}{4t} = 0.8862$$

where t is the length of the side of the equivalent square rod. Thus, for the thermal energy range,

$$\bar{\alpha}_{th} = 0.4431 \left( \frac{\bar{\beta}_{th}}{2-\bar{\beta}_{th}} \right) C_T \qquad (2\text{-}133)$$

In the epithermal energy ranges, $\alpha(E)$ is calculated from Equation (2-129) where $\beta(E)$ is obtained from Figure 2-12 using control rod cross sections from a built-in multigroup library. The group average $\alpha$ is determined by weighting by the flux spectrum at the rod surface. The required flux spectrum is derived in the same way as for the control blade.

$$\phi(E,R_0) = \phi_\infty(E) \left[ \frac{1}{1 - \frac{\alpha}{D\kappa} \frac{\lambda_1(R_0)}{\lambda_2(R_0)}} \right] \qquad (2\text{-}134)$$

where, for a cylindrical rod:

$$\lambda_1(R_0) = \frac{K_1(\kappa R_1)}{I_1(\kappa R_1)} I_0(\kappa R_0) + K_0(\kappa R_0)$$

$$\lambda_2(R_0) = \frac{K_1(\kappa R_1)}{I_1(\kappa R_1)} I_1(\kappa R_0) - K_1(\kappa R_0)$$

and $\kappa = \Sigma_a/D$ is evaluated for the region surrounding the control rod. For practical cases, $\kappa R_0$ is small and $\kappa R_1$ is large, so

$$\lambda_1(R_0) \cong K_0(\kappa R_0)$$

$$\lambda_2(R_0) \cong -K_1(\kappa R_0)$$

Also assuming that $\Sigma_a \cong \Sigma_{tr}$ yields

$$\phi(E,R_0) = \phi_\infty(E) \left[ \frac{1}{1 + \sqrt{3}\ \alpha(E)\ \dfrac{K_0(\kappa R_0)}{K_1(\kappa R_0)}} \right] \tag{2-135}$$

Note that, unlike the control blade, the flux spectrum at the RCC control rod surface is dependent on the external region properties. Thus,

$$\bar{\alpha}_g = \frac{\displaystyle\int_{E_g}^{E_{g+1}} \frac{\alpha(E)\phi_\infty(E)dE}{1 + \sqrt{3}\ \alpha(E)\ \dfrac{K_0(\kappa R_0)}{K_1(\kappa R_0)}}}{\displaystyle\int_{E_g}^{E_{g+1}} \frac{\phi_\infty(E)dE}{1 + \sqrt{3}\ \alpha(E)\ \dfrac{K_0(\kappa R_0)}{K_1(\kappa R_0)}}} \tag{2-136}$$

Now treating the control rod as a diffusive medium instead of an internal boundary, the flux and current distributions in the rod as derived from diffusion theory are:

$$\phi(E,r) = \phi_\infty(E)\ I_0(\kappa r) \tag{2-137}$$

$$J(E,r) = \phi_\infty(E)\ \kappa D\ I_1(\kappa r) \tag{2-138}$$

By definition, the blackness parameter is

$$\bar{\alpha} = \kappa D\ \frac{I_1(\kappa R_0)}{I_0(\kappa R_0)}$$

$$= \sqrt{\Sigma_a D}\ \frac{I_1\left(\sqrt{\dfrac{\Sigma_a}{D}}\ R_0\right)}{I_0\left(\sqrt{\dfrac{\Sigma_a}{D}}\ R_0\right)} \tag{2-139}$$

To determine the control rod absorption cross sections, its diffusion coefficients are assumed to be unity (the reactivity worth of the control rod is insensitive to the diffusion coefficients). Then Equation (2-139) can be solved for $\Sigma_a$ of each group using the appropriate $\bar{\alpha}$: Equation (2-133) for the thermal group and Equation (2-136) for the epithermal groups. Figure 2-14 is a plot of $R_0^2\Sigma_a$ as a function of $R_0\bar{\alpha}$ determined by this method (Reference 2-18).

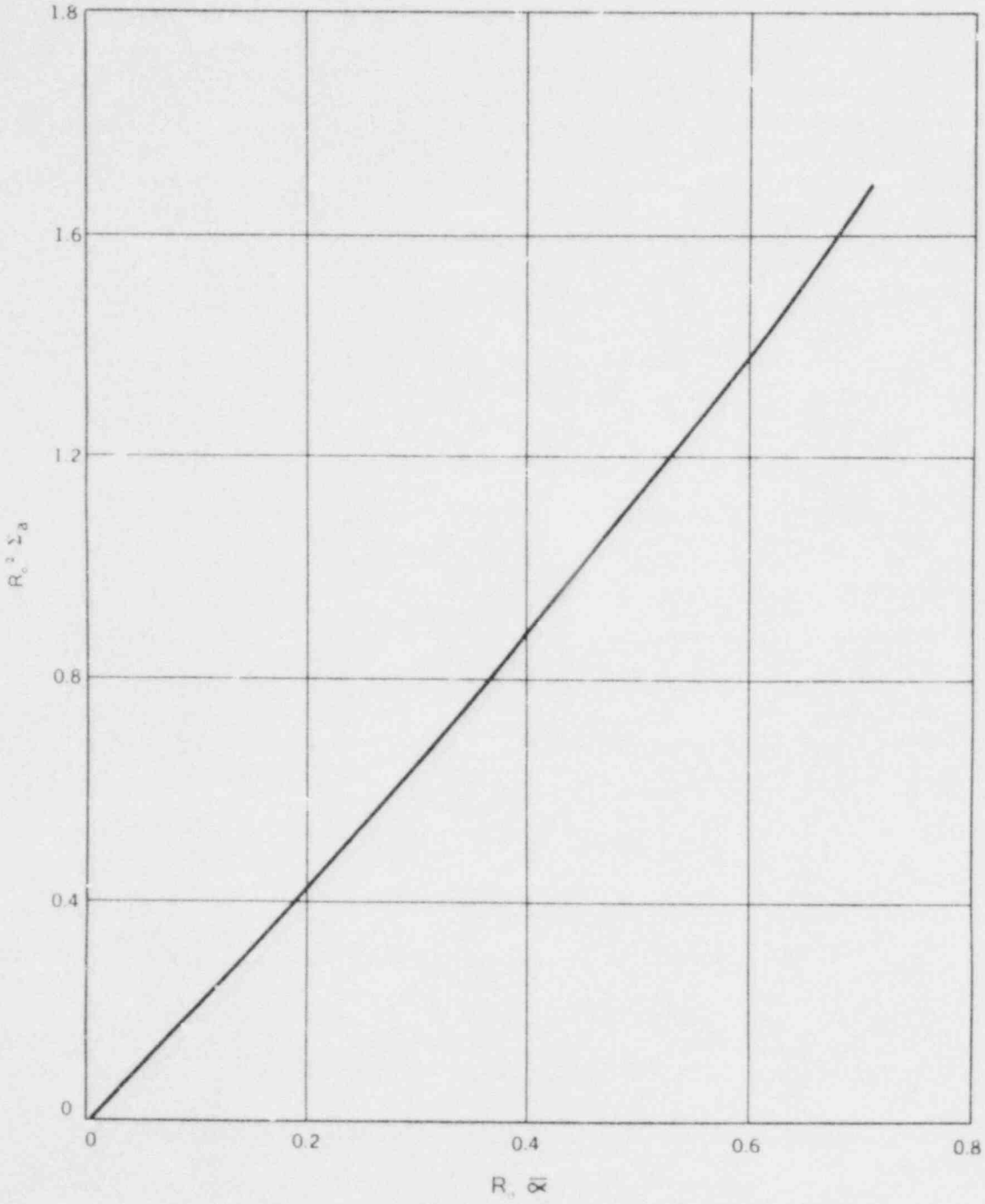


**FIGURE 2-14:** $R_o^2 \Sigma_a$ **VERSUS** $R_o \bar{\alpha}$ **FOR RCC RODS**

## 2.7 FISSION PRODUCT TREATMENT

A modified form of the CINDER point depletion routine is used to calculate the thermal absorption cross section for the lumped fission product. The calculation includes 69 chains consisting of 393 nuclides. Since CINDER is well documented (Reference 2-24), only the modifications to the routine will be discussed.

Average epithermal and thermal fluxes plus fission and absorption cross sections of the fuel nuclides are required to calculate the concentrations of nuclides in the fission product chains. The fluxes are assembly averaged values obtained from the two-dimensional few-group diffusion theory calculation. The epithermal microscopic cross sections are determined by averaging assembly transport theory multigroup values over the broad energy groups. The thermal microscopic cross sections are assembly averaged values determined from Equation (2-85).

The CINDER library contains the thermal cross sections of the fission product chain nuclides at a reference velocity of 2200 m/sec. However, the thermal cross sections used in LATTICE are average values, not 2200 m/sec values. Therefore, the CINDER library cross sections must be modified to appropriately averaged cross sections for the CINDER calculation to be compatible with LATTICE.

The U-235 thermal absorption cross section $\sigma_a^{235}(v_t)$ calculated by LATTICE has the case-dependent spectrum and fuel flux depression effects incorporated into it. Thus, the ratio of $\sigma_a^{235}(v_t)$ to the 2200 m/sec value $\sigma_a^{235}(v_0)$ represents the cross section reduction due to these effects:

$$F = \frac{\sigma_a^{235}(v_t)}{\sigma_a^{235}(v_0)} \qquad (2\text{-}140)$$

This factor can not be applied directly to correct the CINDER cross sections since U-235 is a non-1/v absorber while CINDER assumes 1/v behavior of the nuclides in the fission product chains it represents.

To calculate a correction for the non-1/v behavior of the U-235 cross sections, a LATTICE depletion case was run with a trace amount of B-10, a 1/v absorber, in the fuel pins. The ratio of the effective B-10 thermal absorption cross section to the 2200 m/sec value edited at each depletion step is the total correction factor to be applied to the CINDER cross sections. Comparison of this factor and Equation (2-140) for the same case indicates that Equation (2-140) gives results 10 percent too low. Therefore, the correction factor is adjusted to

$$F = 1.10 \frac{\sigma_a^{235}(v_t)}{\sigma_a^{235}(v_0)} \qquad (2\text{-}141)$$

The above comparison was based on 2200 m/sec cross sections of 694 b for U-235 and 3837 b for B-10.

CINDER uses Equation (2-141) to modify its library cross sections for its calculations, and uses it again to convert the lumped fission product thermal cross section back to the 2200 m/sec reference velocity for use by the rest of LATTICE since computation of the spectra that determines the thermal velocity is repeated for each depletion step. In addition, the epithermal cross section calculated by CINDER is too large because the effect of resonance interaction was neglected (Reference 2-15). A correction factor dependent on H/M is used to reduce the fission product cross section in the epithermal spectrum calculation (Section 2.4).

## CHAPTER 2 REFERENCES


1. J. L. Carter, "HRG3: A Code for Calculating the Slowing-Down Spectrum in the $P_1$ and $B_1$ Approximation," BNWL-1432, 1970.

2. "SUPERTOG - Data Generator: Fine Group Constants and $P_n$ Scattering Matrices from ENDF/B," ORNL-TM-2679, 1973.

3. H. C. Honeck, "THERMOS - A Thermalization Transport Theory Code for Reactor Lattice Calculations," BNL-5826, 1961.

4. N. M. Greene, et. al., "XLACS: A Program to Produce Weighted Multigroup Neutron Cross Sections from ENDF/B," ORNL-TM-3646, 1972.

5. H. C. Honeck and D. R. Finch, "FLANGE-II - A Code to Process Thermal Neutron Data from an ENDF/B Tape," DP-1278, 1971.

6. B. R. Leonard, Jr., et. al., "Cross-Section Standardization for Thermal Power Reactors," EPRI-221, 1975.

7. A. Sauer, "Approximate Escape Probabilities," Nucl. Sci. & Eng., Vol. 16, pp. 519-335, 1963.

8. H. Gellings and A. Sauer, "Description of Dancoff Junior Program," ORNL-tr-4158, 1963.

9. K. M. Case, F. deHoffmann, and G. Placzek, Introduction to the Theory of Neutron Diffusion, Volume 1, Los Alamos Scientific Laboratory, Los Alamos, New Mexico, 1953.

10. J. L. Carter, "HRG3: A Code for Calculating the Slowing-Down Spectrum in the $P_1$ or $B_1$ Approximation, Appendix B," BNWL - 1432, 1970.

11. F. T. Adler, G. W. Hinman, and L. W. Nordheim, "The Quantitative Evaluation of Resonance Integrals," paper No. P/1988, Proceedings of the Second United Nations International Conference on the Peaceful Uses of Atomic Energy, Vol. 16, pp. 155-171, United Nations, Geneva 1958.

12. Y. Ishiguro, "Exact Treatment of the Resonance Absorption of Neutrons of Intermediate Energy," Nuc. Sci. & Eng., Vol. 32, pp. 422-425, 1968.

13. J. Adir and K. D. Lathrop, "Theory of Methods Used in the GGC-3 Multigroup Cross Section Code," GA-7156, 1967.

14. J. L. Carter, "HRG3: A Code For Calculating the Slowing-Down Spectrum in the $P_1$ or $B_1$ Approximation, Appendix A," BNWL - 1432, 1970.

15. R. L. Hellens, "The Physics of PWR Reactors," CONF-720901, pp. 3-22, 1972.

16. H. S. Cheng, C. T. McDaniel, and A. Leonard, "A Nodal Integral Transport Method for Calculation of Two-Dimensional Power Distribution in Non-Uniform Lattices," CONF - 710302, pp. 655-678, 1971.

17. H. C. Honeck, "THERMOS: A Thermalization Transport Theory Code for Reactor Lattice Calculations," BNL-5826, 1961.

18. P. Lemberg, "The RODWORTH Code - A Blackness Theory Calculation of Effective Few Group Diffusion Theory Parameters for Cruciform and RCC Shaped Control Rods," UNC-5228, 1968.

19. M. Michelini, "Neutron Transmission Probabilities Across Control Blades Filled with Round Tubes: Formulation and Accuracy," Nucl. Sci. & Eng., Vol. 42, pp. 162-170, 1970.

20. W. Sha, "An Analysis of Reactivity Worth of the Rod Cluster Control Elements (RCC) and Local Water Hole Power Density Peaking," WCAP-3269-47, 1965.

21. A. F. Henry, "A Theoretical Method for Determining the Worth of Control Rods," WAPD-218, 1959.

22. G. W. Stuart, "Multiple Scattering of Neutrons," Nucl. Sci. & Eng., Vol. 2, pp. 617-625, 1957.

23. G. W. Stuart and R. W. Woodruff, "Method of Successive Generation," Nucl. Sci, & Eng. Vol. 3, pp. 339-373, 1958.

24. T. R. England, "CINDER - A One Point Depletion and Fission Product Program," WAPD-TM-334, 1962.

# 3. TWO-DIMENSIONAL FLUX AND POWER DISTRIBUTIONS

In order to obtain a more accurate calculation of the reactivity of the assembly and the flux distribution for the depletion study, a two-dimensional few-group diffusion theory calculation for the assembly is performed. Then the rod-by-rod relative power distribution is calculated from the flux distribution.

## 3.1 TWO-DIMENSIONAL MULTIGROUP DIFFUSION EQUATIONS

A numerical solution must be found to the diffusion equation for each broad energy group:

$$-\nabla \cdot D(\underline{r})\nabla\phi(\underline{r}) + \Sigma(\underline{r})\phi(\underline{r}) = S(\underline{r}) \tag{3-1}$$

where the space dependent parameters

$D$ = the diffusion coefficient,

$\Sigma$ = the total macroscopic removal cross section,

$\phi$ = the flux distribution, and

$S$ = the source distribution.

The removal cross sections in the nonthermal energy groups include both absorption and scatter out of the group. In two-dimensional rectangular geometry, the diffusion equation is

$$-\frac{\partial}{\partial x}\left(D\frac{\partial\phi}{\partial x}\right) - \frac{\partial}{\partial y}\left(D\frac{\partial\phi}{\partial y}\right) + \Sigma\phi - S = 0 \tag{3-2}$$

To determine the flux distribution, the assembly is divided into an array of mesh points, and Equation (3-2) is integrated over the region associated with each mesh point (the dashed region in Figure 3-1):

$$\iint\left[-\frac{\partial}{\partial x}\left(D\frac{\partial\phi}{\partial x}\right) - \frac{\partial}{\partial y}\left(D\frac{\partial\phi}{\partial y}\right) + \Sigma\phi - S\right]dx\,dy = 0 \tag{3-3}$$

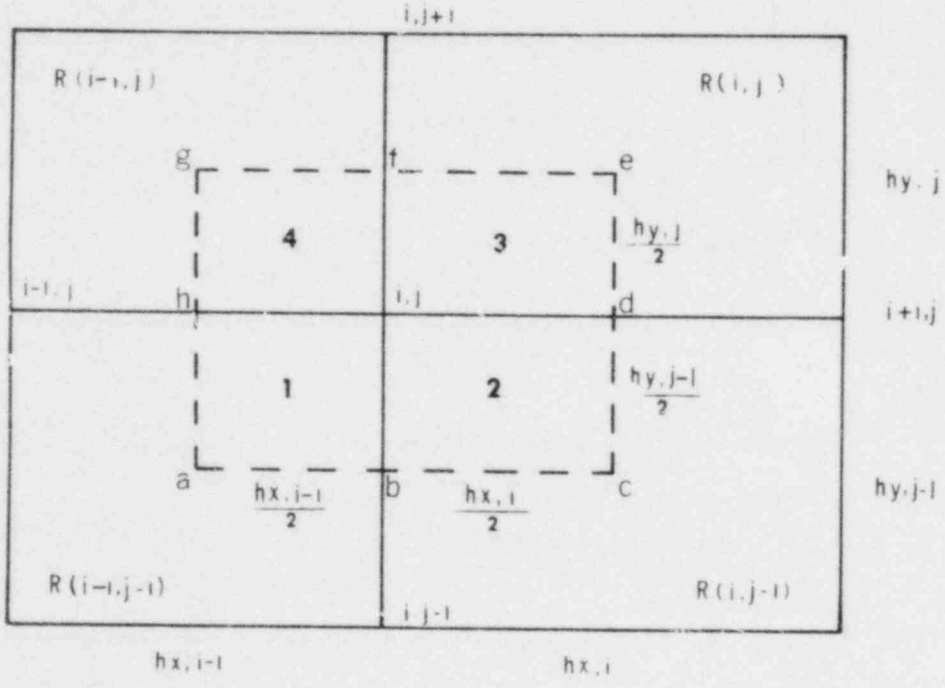


**FIGURE 3-1: MESH FOR THE FIVE-POINT DIFFERENCE EQUATION**

The first two terms can be written as

$$\iint \left[ - \frac{\partial}{\partial x}\left(D\frac{\partial \phi}{\partial x}\right) - \frac{\partial}{\partial y}\left(D\frac{\partial \phi}{\partial y}\right) \right] dx\ dy =$$

$$- \Sigma_{ij}\ D_{ij} \iint \left( \frac{\partial^2 \phi}{\partial x^2} + \frac{\partial^2 \phi}{\partial y^2} \right) dx\ dy \qquad (3\text{-}4)$$

assuming each region R(i,j) is homogeneous and therefore has constant properties. Transform the surface integrals to line integrals using Green's Theorem:

$$\iint \left( \frac{\partial Q}{\partial x} - \frac{\partial P}{\partial y} \right) dx\ dy \ = \ \int_c (P dx + Q dy)$$

Using

$$Q = \frac{\partial \phi}{\partial x} \quad , \quad P = \frac{\partial \phi}{\partial y}$$

yields

$$\iint \left( \frac{\partial^2 \phi}{\partial x^2} + \frac{\partial^2 \phi}{\partial y^2} \right) dx\ dy \ = \int_c \left( - \frac{\partial \phi}{\partial y}\ dx + \frac{\partial \phi}{\partial x}\ dy \right) \qquad (3\text{-}5)$$

Substituting into Equation (3-4) and integrating around the dashed contour in each region gives

$$- \sum_{i,j} D_{ij} \iint \left( \frac{\partial^2 \phi}{\partial x^2} + \frac{\partial^2 \phi}{\partial y^2} \right) dx\ dy = D_{i-i,j-1} \int_a^b \frac{\partial \phi}{\partial y}\ dx + D_{i,j-1} \int_b^c \frac{\partial \phi}{\partial y}\ dx$$

$$- D_{i,j-1} \int_c^d \frac{\partial \phi}{\partial x}\ dy - D_{ij} \int_d^e \frac{\partial \phi}{\partial x}\ dy + D_{ij} \int_e^f \frac{\partial \phi}{\partial y}\ dx \qquad (3\text{-}6)$$

$$+ D_{i-1,j} \int_f^g \frac{\partial \phi}{\partial y}\ dx - D_{i-1,j} \int_g^h \frac{\partial \phi}{\partial x}\ dy - D_{i-1,j-1} \int_h^a \frac{\partial \phi}{\partial x}\ dy$$

Note that the integrals along the contours between regions cancel due to the continuity of current at the material interfaces. Approximating the integrals in Equation (3-6) as

$$\int_A^B \frac{\partial \phi}{\partial y}\, dx = \left(\overline{\frac{\partial \phi}{\partial y}}\right) \Delta x$$

$$\int_A^B \frac{\partial \phi}{\partial x}\, dy = \left(\overline{\frac{\partial \phi}{\partial x}}\right) \Delta y$$

with a backward difference for the average derivatives, Equation (3-6) becomes

$$- \sum_{i,j} D_{ij} \iint \left(\frac{\partial^2 \phi}{\partial x^2} + \frac{\partial^2 \phi}{\partial y^2}\right) dx\, dy = \tag{3-7}$$

$$a_{ij}\, \phi_{i+1,j} + a_{i-1,j}\, \phi_{i-1,j} + b_{ij}\, \phi_{ij} + c_{ij}\, \phi_{i,j+1} + c_{i,j-1}\, \phi_{i,j-1}$$

where

$$a_{ij} = - \frac{1}{2h_{x,i}} \left(D_{i,j-1}\, h_{y,j-1} + D_{ij}\, h_{y,j}\right)$$

$$c_{ij} = - \frac{1}{2h_{y,j}} \left(D_{ij}\, h_{x,i} + D_{i-1,j}\, h_{x,i-1}\right)$$

$$b_{ij} = - \left(a_{ij} + a_{i-1,j} + c_{ij} + c_{i,j-1}\right)$$

The last two terms of Equation (3-3) are

$$\iint (\Sigma\phi - S)\, dx\, dy = \sum_{i,j} \left(\Sigma_{ij} \iint \phi\, dx\, dy - \iint S\, dx\, dy\right) \tag{3-8}$$

The integrals can be approximated by

$$\iint \phi\, dx\, dy = \phi_{ij}\, \Delta x \Delta y$$
$$\iint S\, dx\, dy = \bar{S}_{ij}\, \Delta x \Delta y$$

where $\phi_{ij}$ and $\bar{S}_{ij}$ represent averages in region R(i,j). Then Equation (3-8) can be written as

$$\sum_{i,j} \left(\Sigma_{ij} \iint \phi\, dx\, dy - \iint S\, dx\, dy\right) = b'_{ij} \phi_{ij} + f_{ij} \tag{3-9}$$

where

$$b'_{ij} = \frac{h_{x,i}}{2}\left(\frac{\Sigma_{ij}\, h_{y,j}}{2} + \frac{\Sigma_{i,j-1}\, h_{y,j-1}}{2}\right) + \frac{h_{x,i-1}}{2}\left(\frac{\Sigma_{i-1,j}\, h_{y,j}}{2} + \frac{\Sigma_{i-1,j-1}\, h_{y,j-1}}{2}\right)$$

$$f_{ij} = -\frac{h_{x,i}}{2}\left(\frac{\bar{S}_{ij}\, h_{y,j}}{2} + \frac{\bar{S}_{i,j-1}\, h_{y,j-1}}{2}\right) - \frac{h_{x,i-1}}{2}\left(\frac{\bar{S}_{i-1,j}\, h_{y,j}}{2} + \frac{\bar{S}_{i-1,j-1}\, h_{y,j-1}}{2}\right)$$

The five-point difference form of Equation (3-3) is the sum of Equations (3-7) and (3-9):

$$a_{ij}\,\phi_{i+1,j} + a_{i-1,j}\,\phi_{i-1,j} + b''_{ij}\,\phi_{ij} + c_{ij}\,\phi_{i,j+1} + c_{i,j-1}\,\phi_{i,j-1} + f_{ij} = 0 \qquad (3\text{-}10)$$

where $b''_{ij} = b_{ij} + b'_{ij}$

Equation (3-10) is solved for each group, but the form of the source is dependent on the group. If all fission neutrons are born in the highest energy group, and if only downscattering between groups is allowed, then the average source for group g in each region can be written as

$$\bar{S}^{g}_{ij} = \begin{cases} \frac{1}{k}\sum_{g=1}^{G} \upsilon\Sigma^{g}_{f_{ij}}\,\phi^{g}_{ij} & g = 1 \qquad (3\text{-}11a) \\ \Sigma^{g-1}_{r_{ij}}\,\phi^{g-1}_{ij} & g \neq 1 \qquad (3\text{-}11b) \end{cases}$$

where

G = the number of energy groups,

k = the multiplication factor of the assembly,

$\upsilon\Sigma^{g}_{f_{ij}}$ = the macroscopic nu-fission cross section for group g in region R(i,j), and

$\Sigma_{r_{ij}}^{g-1}$ = the macroscopic removal cross section out of group g-1 into group g in region R(i,j).

Examination of Equation (3-10) and its associated coefficients indicates that parameters for a non-existent region external to the system boundary are required to calculate the flux at the boundary. Mirror (zero-current) boundary conditions are assumed:

$$\left.\frac{\partial\phi}{\partial x}\right|_{S_x} = 0 \quad , \quad \left.\frac{\partial\phi}{\partial y}\right|_{S_y} = 0$$

hence the properties of the imaginary region must be chosen so that the above conditions are satisfied when Equation (3-10) is solved for points on the boundary. The simplest choice for such an external medium is a vacuum. Then all required external region material properties for the calculation of the coefficients in Equation (3-10) on the boundary are zero. The coefficient of the flux outside the boundary becomes zero, eliminating the outside flux from the equation. Therefore, the external flux can be set equal to zero and the coefficient need not be calculated. The other coefficients now depend only on regions within the boundary. Since each term in a coefficient is the product of a region material property and that region's mesh spacing, the external region mesh spacing can also be set equal to zero. Thus any material properties may be used for the imaginary region with the same results.

## 3.2 METHOD OF SOLUTION

Since the fission source, Equation (3-11a), is a function of the flux, a two part iteration scheme is necessary to solve the coupled set of equations formed from Equation (3-10). The fission source is held constant during inner iterations on the flux and then recalculated using the converged flux in the outer iteration to begin the process again.

To begin the calculation, an initial guess of k and the flux for each group is required. The fission source is calculated and the inner iterations for the highest energy group are performed. Then the inner iterations are repeated for the lower energy groups using the slowing down source, Equation (3-11b). A new estimate of k is made:

$$k = \frac{\sum_{i,j,g} \upsilon \Sigma_{f_{ij}}^{g} \phi_{ij}^{g}}{\sum_{i,j,g} \Sigma_{a_{ij}}^{g} \phi_{ij}^{g}}$$

to recalculate the fission source. The process is repeated until both k and the flux converge.

In the inner iterations, the alternating direction implicit method (Reference 3-1) is used to solve the matrix of mesh equations obtained from Equation (3-10). First the equations are solved in the i direction using the results from the previous iteration to get an intermediate value of the flux. Then this intermediate flux is used to solve the equations in the j direction to get the new flux and complete the iteration.

In the nth iteration, for the i direction sweeps, Equation (3-10) can be rewritten in tridiagonal form by combining the constant terms:

$$a_{i-1,j}\,\phi^{n-\frac{1}{2}}_{i-1,j} + b''_{ij}\,\phi^{n-\frac{1}{2}}_{ij} + a_{ij}\,\phi^{n-\frac{1}{2}}_{i+1,j} + g^{n-1}_{ij} = 0 \qquad (3\text{-}13)$$

where

$$g^{n-1}_{ij} = c_{i,j-1}\,\phi^{n-1}_{i,j-1} + c_{ij}\,\phi^{n-1}_{i,j+1} + f_{ij}$$

and $\phi^{n-\frac{1}{2}}$ is the intermediate flux. Equation (3-13) is solved by Gaussian elimination for each value of j. Substituting the intermediate flux into Equation (3-10) gives the equation for the j direction:

$$c_{i,j-1}\,\phi^{n}_{i,j-1} + b''_{ij}\,\phi^{n}_{ij} + c_{ij}\,\phi^{n}_{i,j+1} + g^{n-\frac{1}{2}}_{ij} = 0 \qquad (3\text{-}14)$$

where

$$g^{n-\frac{1}{2}}_{ij} = a_{i-1,j}\,\phi^{n-\frac{1}{2}}_{i-1,j} + a_{ij}\,\phi^{n-\frac{1}{2}}_{i,j+1} + f_{ij}$$

Equation (3-14) is solved for each value of i to determine the new flux estimate $\phi^{n}$. Between iterations, the value of the flux is modified using linear acceleration in order to improve convergence:

$$\phi^{n\,\prime} = \phi^{n-1} + \delta(\phi^{n} - \phi^{n-1}) \qquad (3\text{-}15)$$

where $\delta$ is the over-relaxation parameter.

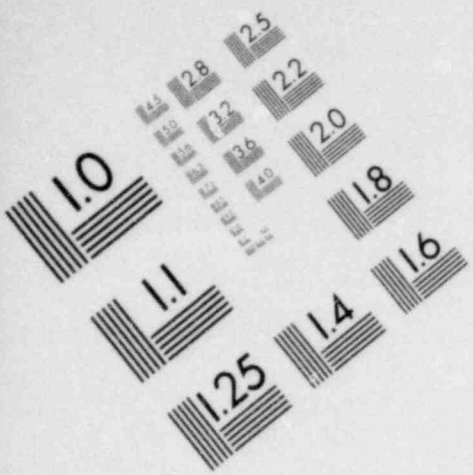


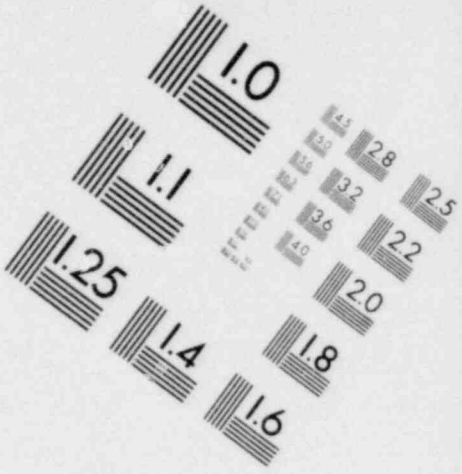


**IMAGE EVALUATION**
**TEST TARGET (MT-3)**

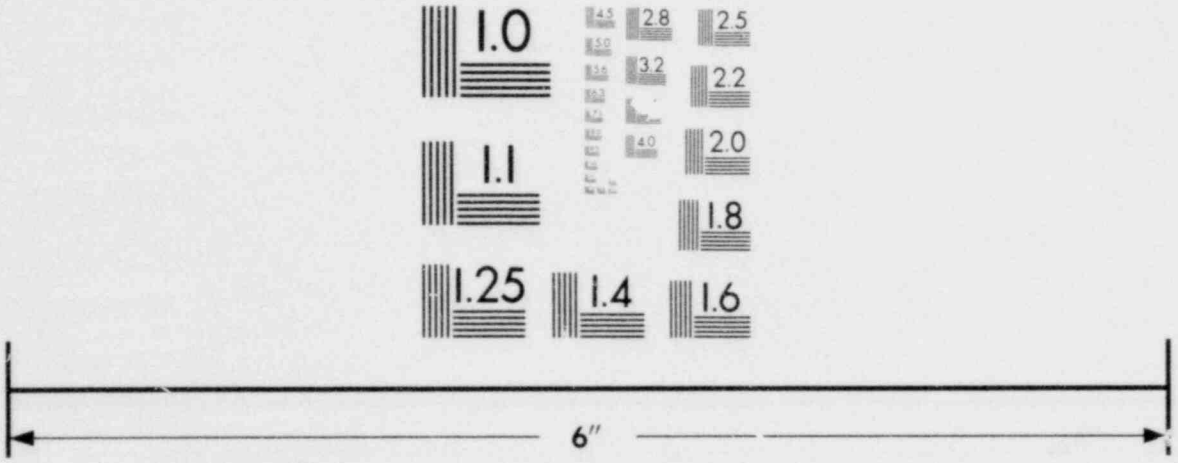


**MICROCOPY RESOLUTION TEST CHART**

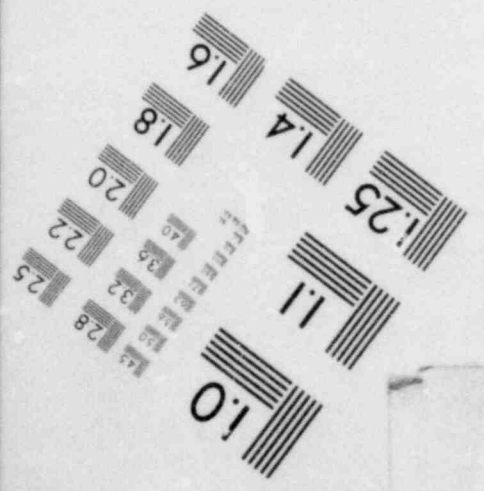


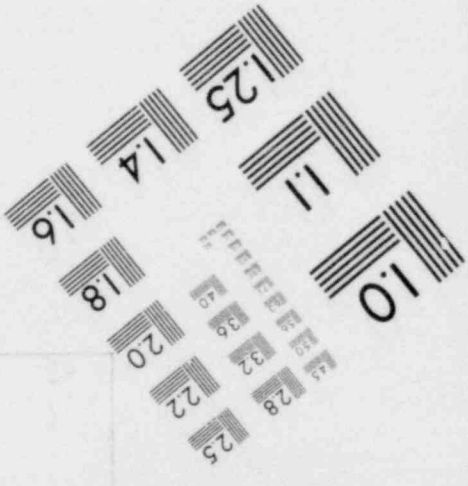

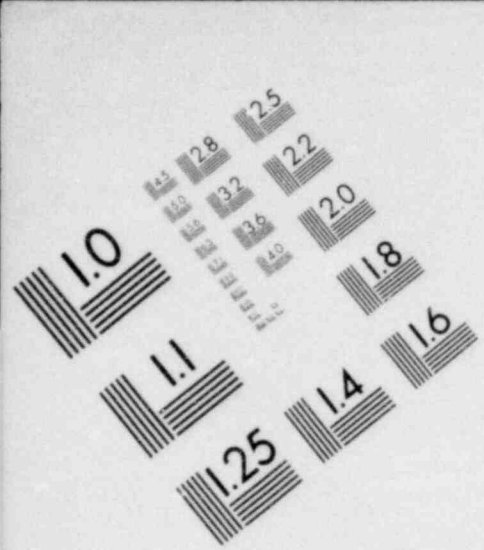


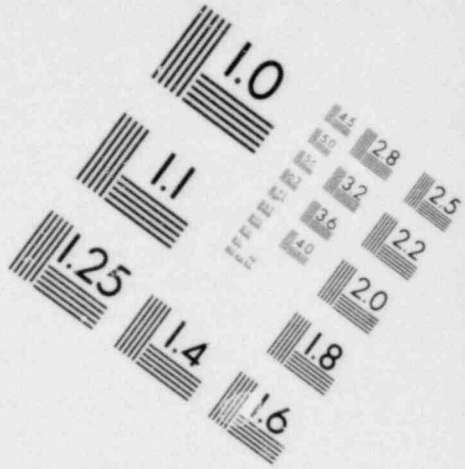


**IMAGE EVALUATION**
**TEST TARGET (MT-3)**

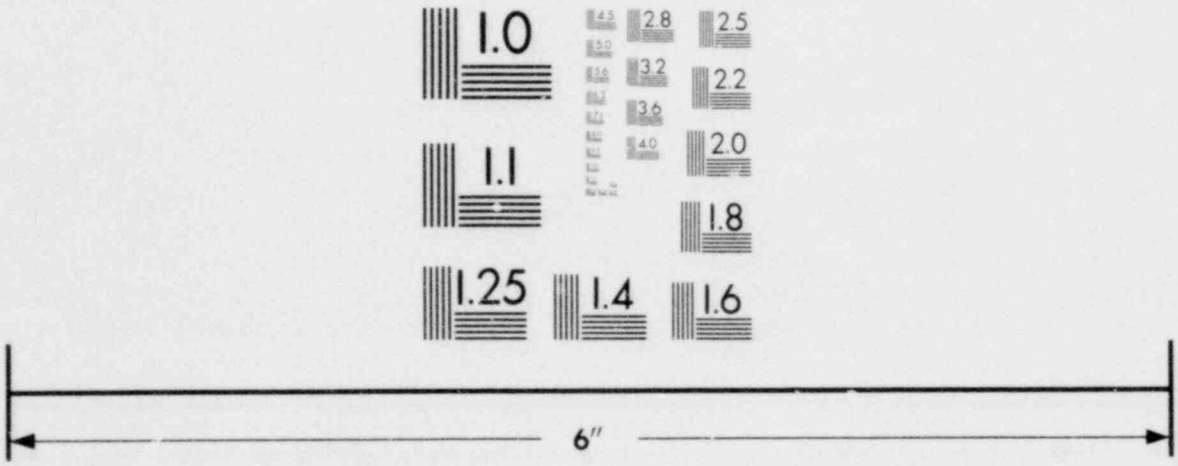


**MICROCOPY RESOLUTION TEST CHART**

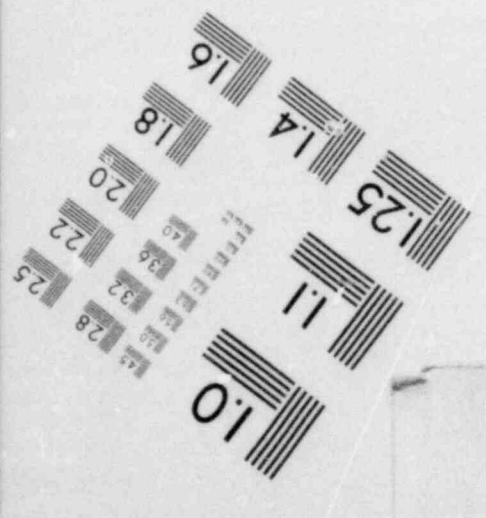


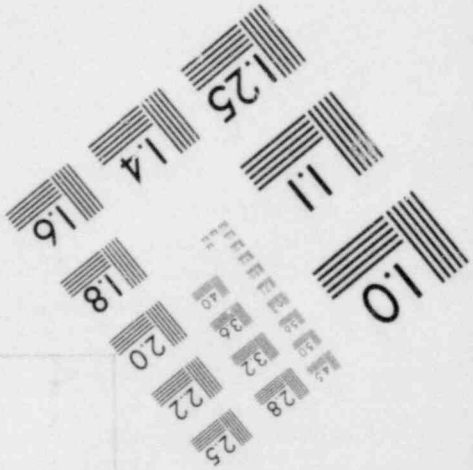

## 3.3 RELATIVE POWER DISTRIBUTION

The rod-by-rod relative power distribution in the assembly can be calculated after the two-dimensional flux distribution has been determined as outlined above. Neglecting the contribution of the gamma ray source, the rod power is proportional to the fission rate in the cell·

$$P_i = V_i \sum_{g=1}^{G} \sum_{n=1}^{N} \kappa_n \Sigma_{f_{ni}}^{g} \phi_i^g \qquad (3\text{-}16)$$

where

$V_i$ = the volume of cell i,

$\kappa_n$ = the energy release per fission in nuclide n,

$\Sigma_{f_{ni}}^{g}$ = the cell macroscopic fission cross section of nuclide n, in group g, and

$\phi_i^g$ = the cell average flux in group g.

The relative power is obtained by dividing by the average rod power of the assembly:

$$\bar{P}_i = \frac{P_i}{\frac{1}{I} \sum_{i=1}^{I} P_i} \qquad (3\text{-}17)$$

where I is the number of fuel rods in the assembly.

## 3.4 MESH DESCRIPTION

The model used for a typical BWR assembly with the control rod inserted is shown in Figure 3-2. Each region boundary corresponds to a mesh line; additional mesh lines are included to improve the accuracy of the calculation.

All lattice locations are treated as separate regions because of the differences in spectrum and composition. Cells containing burnable poison are divided into a discrete pellet region surrounded by homogenized moderator and cladding. In non-burnable poison cells, the fuel, cladding, and moderator are homogenized into one region with two additional mesh lines within the region. As an option, the fuel cells can be modeled the same way as burnable poison cells. Extra in-channel water not associated with the unit cells is included in the cells adjacent to the channel.

The channel is homogenized into the water gaps outside the assembly. Each of these regions has two equally spaced internal mesh lines except in the control rod slot when the control blade is present. Then the two mesh lines are spaced to coincide with the blade structure (Figure 3-2).

The symmetry of a typical PWR assembly allows the use of a one-quarter assembly model (Figure 3-3), but the option to model a full assembly is retained. The burnable poison cells are treated the same way as for a BWR, and the control rods are modeled the same way as burnable poison rods. The homogenized fuel cells have one internal mesh line instead of two except when a burnable poison or control rod cell is in the same row and/or column. Since the control rods are within the lattice, the water gap between the assemblies is narrow and requires no internal mesh lines.

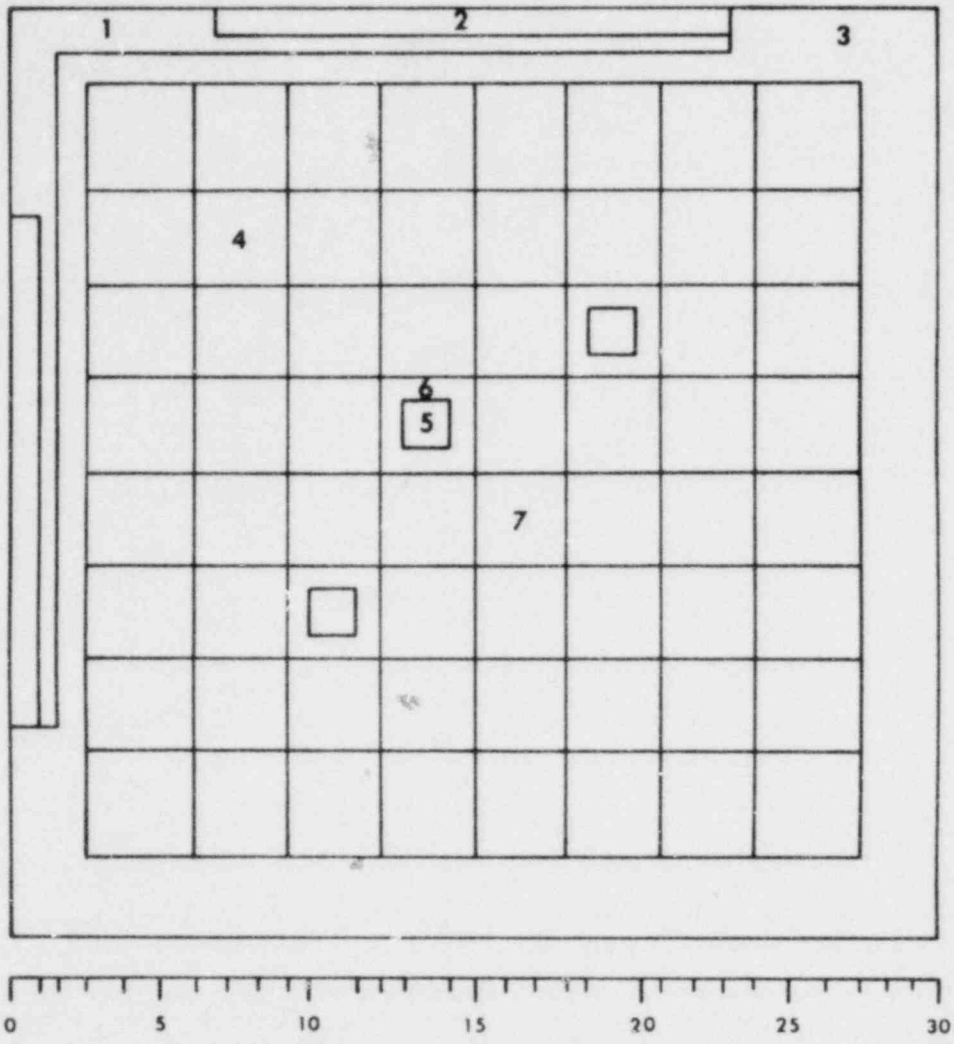


1 – CONTROL BLADE STRUCTURE

2 – ACTIVE CONTROL BLADE

3 – HOMOGENIZED EX-CHANNEL WATER AND CHANNEL

4 – HOMOGENIZED FUEL CELL

5 – BURNABLE POISON

6 – HOMOGENIZED MODERATOR AND CLADDING

7 – WATER HOLE

FIGURE 3–2: MODEL FOR BWR ASSEMBLY

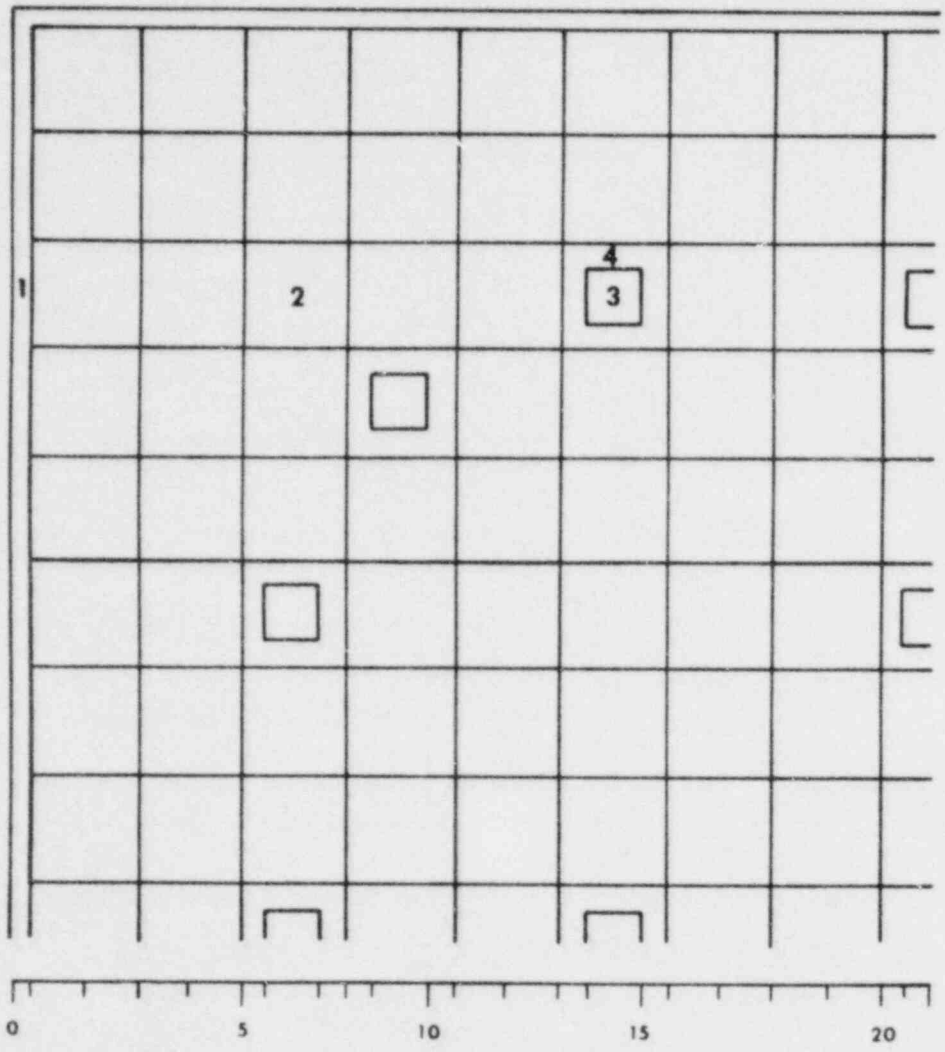


1 – WATER GAP

2 – HOMOGENIZED FUEL CELL

3 – BURNABLE POISON OR CONTROL ROD

4 – HOMOGENIZED MODERATOR AND CLADDING

FIGURE 3-3: MODEL FOR ¼ PWR ASSEMBLY

## CHAPTER 3 REFERENCE

1. D. W. Peaceman and H. H. Rachford, Jr., "The Numerical Solution of Parabolic and Elliptic Differential Equations," J. of Soc. Indust. Appl. Math., Vol. 3, pp. 28-41, 1955.

# 4. DEPLETION CALCULATIONS

The lattice physics methods which have previously been described apply only to a fixed point in time. However, during operation of the reactor, the fuel concentrations in the lattice change and the concentrations of strongly absorbing fission products increase. The changes in the nuclei concentrations are accounted for by solving the depletion equations. The basic assumptions used in solving these equations are that the power density and the activation rates (absorption, fission and capture) remain constant during the time step.

## 4.1 ISOTOPIC DEPLETION EQUATIONS

The depletion equations are a coupled set of first order differential equations which describe the variation with time of the number densities of the nuclei in the lattice. The time rate of change in the concentration of nuclide i at position r can be expressed in terms of "source strengths", $s_{ij}$, and an "absorption strength", $a_i$:

$$\frac{d}{dt} N_i(r,t) = \sum_{j=1}^{M} s_{ij}(r)N_j(r,t) - a_i r)N_i(r,t) \quad i = 1,2,\ldots,M \tag{4-1}$$

where $N_i(r,t)$ is the concentration of nuclide i at time t and position r and M is the maximum number of nuclei.

The source strength of a nuclide i from nuclide j is the sum of contributions from all possible mechanisms, i.e., fission, decay, and neutron-capture. Thus the general expression for the source strength may be written as

$$s_{ij}(r) = Y_{j\rightarrow i} A_j^f(r) + \lambda_{ij} + A_j^c(r) \tag{4-2}$$

where

$\nu_{j\to i}$ = the yield of nuclide i from the fissioning of nuclide j,

$A_j^f = \sum_g \sigma_{f,j}^g \phi^g$, the fission activation rate,

$\sigma_{f,j}^g$ = the microscopic fission cross section of nuclide j in group g,

$\phi^g$ = the flux in group g,

$\lambda_{ij}$ = the decay constant for production of nuclide i from the decay of nuclide j, and

$A_j^c = A_j^a - A_j^f$, the capture activation rate where $A_j^a$ is an absorption rate analogous to $A_j^f$.

The absorption strength of a nuclide i is the sum of its absorption rate and decay constant:

$$a_i(r) = A_i^a(r) + \lambda_i \tag{4-3}$$

A schematic diagram of the depletion chains that are used is given in Figure 4-1. Note that the short lived and low cross section stages are neglected. Also only the fission products with large macroscopic absorption cross sections are included explicity while the rest are lumped into a single pseudo fission product (see Section 2.7).

## 4.2 METHOD OF SOLUTION

To solve the depletion equations, Equation (4-1), the assumption is made that the activation rates (and thus the absorption and source strengths) are constant through the time step. Therefore the solution to Equation (4-1) is

$$N_i(t) = N_i(0)e^{-a_i t} + e^{-a_i t}\int_0^t e^{a_i \tau}\sum_{j=1}^{M} s_{ij}N_j(\tau)d\tau \tag{4-4}$$

1. Depletion Chain for U-235

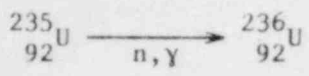


2. Depletion Chain for U-238

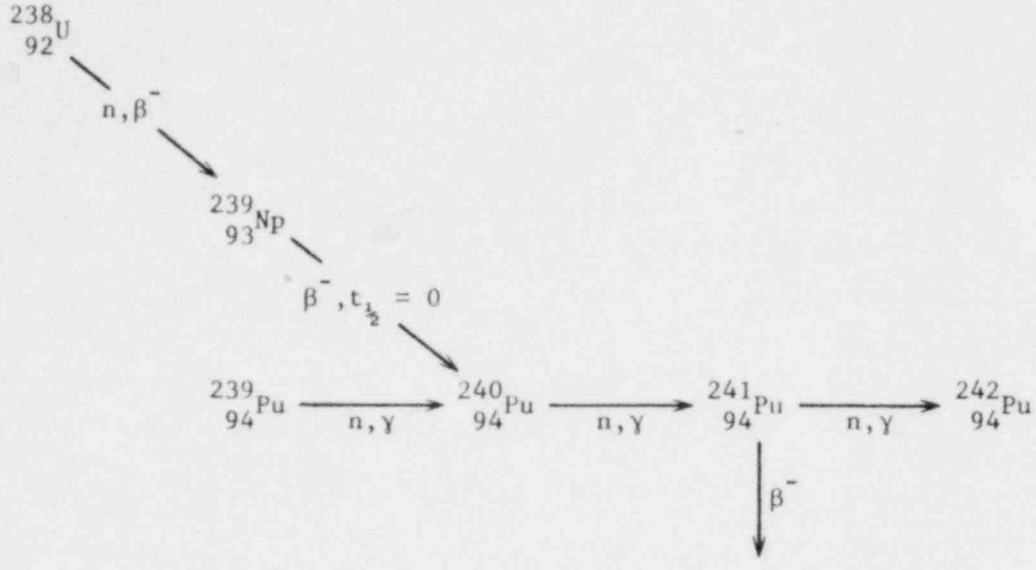


3. Depletion Chain for Gd-154

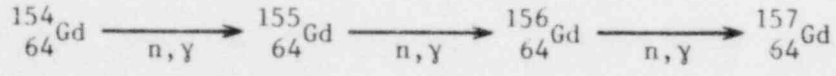


4. Fission Product Chains

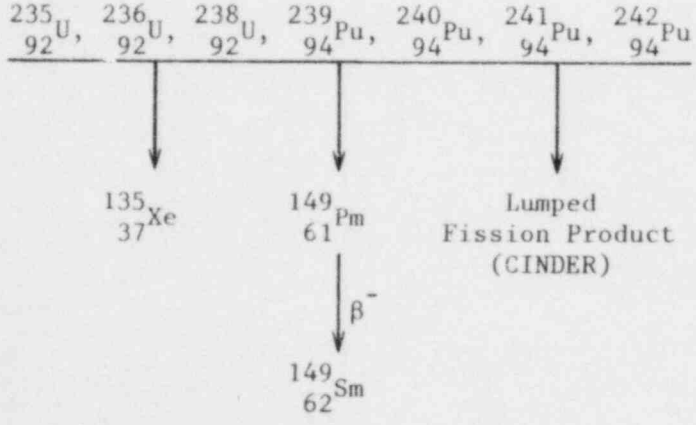


FIGURE 4-1: DEPLETION CHAINS REPRESENTED

where for simplicity the spatial dependence has been neglected. In practice, each fuel pin is treated as a separate depletable region which may have a different isotopic content.

The solution to the depletion equations may be divided into two parts: the homogeneous part as indicated by the first term of the right-hand side of Equation (4-4) and the inhomogeneous part which represents the contribution of the sources as the second term of the right-hand side of Equation (4-4). Since the depletion equations are linear in the source terms, the contribution from each source $s_{ij}N_j$ may be calculated independently of the other sources.

For the first nuclide in a depletion chain there are no sources; thus the homogeneous part of Equation (4-4) is the complete solution:

$$N_1(t) = N_1(0)e^{-a_1 t} \tag{4-5}$$

In continuing to solve the equations, use is made of depletion functions in a manner similar to that described in Reference 4-1. Defining the first depletion function as

$$F_1(x) = e^{-x} \tag{4-6}$$

Equation (4-5) may be written as

$$N_1(t) = N_1(0)\cdot F_1(a_1 t) \tag{4-7}$$

For the second nuclide $N_2$ in a depletion chain with nuclide $N_1$ as source, the homogeneous part of Equation (4-4) is

$$N_2^{hom}(t) = N_2(0)\cdot F_1(a_2 t) \tag{4-8}$$

and the inhomogeneous part due to the contribution of the source $s_{21}N_1(t)$ is

$$N_2^{in}(t) = e^{-a_2 t} \int_0^t e^{a_2 \tau} s_{21} N_1(\tau) d\tau$$

$$= e^{-a_2 t} \int_0^t e^{a_2 \tau} s_{21} N_1(0) F_1(a_1 \tau) d\tau$$

$$= N_1(0) \cdot s_{21} \cdot \frac{e^{-a_1 t} - e^{-a_2 t}}{a_2 - a_1}$$

$$= N_1(0) \cdot s_{21} t \cdot \frac{F_1(a_1 t) - F_1(a_2 t)}{a_2 t - a_1 t} \qquad (4\text{-}9)$$

Defining the second depletion function as

$$F_2(x_1, x_2) = \frac{F_1(x_1) - F_1(x_2)}{x_2 - x_1} \qquad (4\text{-}10)$$

Equation (4-9) becomes

$$N_2^{in}(t) = N_1(0) \cdot s_{21} t \cdot F_2(a_1 t, a_2 t) \qquad (4\text{-}11)$$

Therefore the complete solution for the second nuclide in a chain with a single source $s_{21} N_1$ is

$$N_2(t) = N_2^{hom}(t) + N_2^{in}(t)$$

$$= N_2(0) \cdot F_1(a_2 t) + N_1(0) \cdot s_{21} t \cdot F_2(a_1 t, a_2 t) \qquad (4\text{-}12)$$

For M different sources $s_{2j} N_j$ the general solution is

$$N_2(t) = N_2(0) \cdot F_1(a_2 t) + \sum_{j=1}^{M} N_j(0) \cdot s_{2j} t \cdot F_2(a_j t, a_2 t) \qquad (4\text{-}13)$$

Consider now the third nuclide $N_3$ in a depletion chain with the second nuclide $N_2$ as the source. Using Equation (4-12) with Equation (4-4) yields

$$N_3(t) = N_3(0) \cdot F_1(a_3 t) + e^{-a_3 t} \int_0^t e^{a_3 \tau} s_{32} N_2(\tau) d\tau$$

$$= N_3(0) \cdot F_1(a_3 t) + N_2(0) \cdot s_{32} t \cdot F_2(a_3 t, a_2 t) +$$

$$N_1(0) \cdot s_{21} t \cdot s_{32} t \cdot F_3(a_3 t, a_2 t, a_1 t) \qquad (4\text{-}14)$$

where $F_3(x_1,x_2,x_3)$ is the third depletion function, defined below.

Likewise it can be shown that for the k-th nuclide in a depletion chain with the (k-1)-th nuclide as source, the solution to the depletion equation is (Reference 4-1)

$$N_k(t) = \sum_{j=1}^{k} N_j(0) \cdot F_{k+1-j}(a_k t,\ldots,a_1 t) \cdot \prod_{i=j}^{k-1} (s_{ij} t) \qquad (4\text{-}15)$$

For cases where there are more than one source term between some of the nuclei in the chain, new chains have to be created following the new sources, and the contributions from all the branches of the different chains are added to get the general solution for each nuclide as was done for k = 2 [Equation (4-13)].

In evaluating the depletion functions use is made of the recurrence relation (Reference 4-1)

$$F_k(x_k,x_{k-1},\ldots,x_1) = \frac{F_{k-1}(x_k,\ldots,x_3,x_1) - F_{k-1}(x_k,\ldots,x_3,x_2)}{x_2 - x_1} \qquad (4\text{-}16)$$

for $k \geq 2$.

It should be noted that in evaluating the depletion functions, the numerator and denominator of one of the functions may become small at the same time, thereby resulting in loss of information. To combat this possibility a series expansion for the exponentials is used:

$$e^x = \sum_{n=0}^{\infty} \frac{x^n}{n!}$$

Using this expansion the second and third depletion functions become

$$F_2(x_2,x_1) = F_1(x_2) \sum_{n=1}^{\infty} \frac{(x_2-x_1)^{n-1}}{n!} \qquad (4\text{-}17)$$

$$F_3(x_3,x_2,x_1) = F_1(x_3) \frac{1}{x_2-x_1} \sum_{n=1}^{\infty} \frac{1}{n!} \left[(x_3-x_1)^{n-1} - (x_3-x_2)^{n-1}\right] \qquad (4\text{-}18)$$

Also, in order to avoid other numerical problems, the fission products which have large absorption cross sections or decay constants are treated as though their concentrations were in steady state. The steady state condition implies that the time rate of change in the nuclide density is zero:

$$\frac{d}{dt} N_i(t) = 0 \tag{4-19}$$

Then Equation (4-1) can be solved using Equation (4-3)

$$N_i(t) = \frac{\sum_{j=1}^{M} s_{ij} N_j(t)}{A_i^a + \lambda_i} \tag{4-20}$$

The depletion equations are solved at the end of each time step. Due to the high absorption rate in the burnable poison pins, a predictor-corrector method is used to obtain a better estimate of the burnable poison number densities. For each time step the thermal neutron spectrum and flux distribution calculations are repeated. However, because of the slow change in the fast spectrum with exposure, the fast spectrum and flux distribution calculation is repeated only when the exposure interval from the previous fast calculation reaches a predetermined value.

## 4.3 NORMALIZATION

The depletion equations are solved for the fuel or super cell representing each spectrum region in the one-dimensional transport calculations to account for spectrum effects and the radial dependence of the nuclide concentrations across the cell. Each pin is depleted separately in the two-dimensional calculation of the assembly to determine average cell concentrations which include the effect of interaction

of the pin with other assembly regions. For the results of these calculations to be consistent, they must be normalized to one another. Since the two-dimensional depletion more accurately models the conditions in the pins, the one-dimensional cell results are normalized to agree with the assembly calculation.

The normalization of the one-dimensional results is in three parts. First the activation rates for each cell are normalized to the average activation rates calculated for the time step by two-dimensional diffusion theory for the pins in the spectrum region represented by the cell. Then the depletion equations are solved.

Further normalization of the activation rates is required since the power density $P_0$ is assumed to be constant. The power density is defined as

$$P_0 \equiv \sum_{i=1}^{M_F} \kappa_i N_i(t) A_i^f \qquad (4\text{-}21)$$

where

$M_F$ = the number of fissionable nuclei,

$\kappa_i$ = the energy released per fission of nuclide i, and

$A_i^f = \sum_g \sigma_{f,i}^g \phi^g$, the fission activation rate for nuclide i.

Since the nuclide concentrations changed and the activation rates were assumed constant during the depletion step, the power density is no longer the same as it was before the depletion. Therefore, the absorption and fission activation rates are normalized by the ratio of the power before depletion $P_0$ and the power after depletion $P_t$:

$$A_i^k(t) = A_i^k(0) \frac{P_0}{P_t} \quad , \quad k = a,f \qquad (4\text{-}23)$$

This completes the normalization of the activation rates; however, the nuclide concentrations must also be normalized. This is done in a similar manner as the first normalization of the cell activation rates. The nuclide concentrations from the assembly depletion are assumed to be correct and the cell concentrations are normalized so that they match the average values for the pins in the spectrum region represented by the cell. Once these normalizations have been completed, the two sets of depletion calculations are consistent.

## CHAPTER 4 REFERENCE

1. H. Siewers, "An Analytical Method for Solving Depletion Equations," Atomkernenergie (ATKE) Bd. 27, Lfg. 1, pp. 30-34, 1976.